# Evaluating Embedded Heater Bonding for Composites

Casey Carte

A thesis
Submitted in partial fulfillment of the
Requirements for the degree of

Master of Science in Mechanical Engineering

University of Washington

2017

Committee:
Santosh Devasia
Mark Tuttle
Mahdi Ashrafi

Program Authorized to Offer Degree:
Mechanical Engineering

University of Washington

**Abstract**

Evaluating Embedded Heater Bonding for Composites

Casey Carte

Chair of the Supervisory Committee:
Prof. Santosh Devasia, Prof. Mark Tuttle
Mechanical Engineering

Out-of-autoclave bonding of high-strength carbon-fiber composites structures can reduce costs associated with autoclaves. Nevertheless, a concern is whether out-of-autoclave bonding results in a loss of delamination toughness. The main contribution of this paper is to comparatively evaluate the delamination toughness of adhesively bonded composite parts using carbon fiber embedded heaters and those bonded in an autoclave. Carbon Fiber Reinforced Polymer (CFRP) adherends were bonded by passing an electrical current through a layer of carbon fiber prepreg embedded at the bondline between two electrically insulating thin film adhesives. The delamination toughness was evaluated under mode I dominated loading conditions using a modified single cantilever beam test. Experimental results show that the delamination toughness of specimens bonded using a carbon fiber embedded heater was comparable to that of samples bonded in an autoclave.

TABLE OF CONTENTS

Page

# LIST OF FIGURES

# ACKNOWLEDGEMENTS

This work was financially supported by NSF Grant CMMI 1536306 and the Nisqually Tribe. The author would also like to thank Brandon Smith and Mahdi Ashrafi for their insightful input and Prof. Santosh Devasia and Prof. Mark Tuttle for their support.

# CHAPTER 1

## INTODUCTION

Composites usually have a better strength to weight ratio and stiffness-to-weight ratio than traditional materials [1]. Carbon Fiber Reinforced Polymers (CFRPs) are being used increasingly in numerous industries including aircraft, space, automotive, sporting goods, and marine industries [2]. Bonding large CFRP components, e.g., stringers and skin of an aircraft wing, requires ever-larger, expensive autoclaves to cure the adhesive between the adherends being joined. Nevertheless, adhesive bonding is preferred over mechanical fastening (such as bolts) when the additional weight of the fasteners is not acceptable, e.g., in transportation applications where the increased weight can increase operating costs. Moreover, drilling holes in the composite (for the fasteners) can cause delamination and reduce the strength of the parts being joined [3]. The adherends are often joined in a large autoclave to cure the thin layer of adhesives at the bondline between the adherends. However, the use of autoclaves in bonding is not efficient (in terms of time and cost) since the entire structure needs to be heated to cure the thin layer of adhesive at the bondline. This motivates the development of out-of-autoclave, more localized-heating techniques for bonding composites.

A challenge with typical localized-heating methods, such as a heat blanket or heat lamps at the surface of the adherends, is that the heat needs to be transferred to the adhesive at the bondline through the composite adherends. However, since the CFRP typically have poor thermal conductivity, the temperature at the surface of the adherend must be higher than at the bondline when using external heating elements, which can potentially damage the part [1]. Moreover, the temperature at the bondline could be uneven due to differing thermal conduction

(e.g., because of varying adherend thickness) leading to uneven curing of the adhesive at the bondline [4]. This challenge of transferring heat from the surface to the bondline is addressed by techniques that aim to generate heat at the bondline. One method is to use UV photo-curable adhesives that can be used with glass fiber adherends that allow the transfer of UV light to the bondline [5]. However, this can prove challenging to extend to carbon fiber adherends, since carbon fibers are not UV transparent [6]. Another method is to use inductive heating to cure epoxy adhesive for composite parts. While it has been shown that this method produces strong bonds [4], edge and local heating effects which can cause uneven bondline temperatures have caused problems with large scale implementations [7]. Curing composites with microwaves has been explored as well, but the heating efficiency is dependent on the dielectric properties of the material which limits the type of resin system or adhesive that can be used [8] [9] [10].

This paper evaluates an out-of-autoclave bonding method using an embedded resistance heater, which applies heat at the bondline to cure the adhesives. In this method, a layer of carbon fiber prepreg with an electrically insulating thin film adhesive on each side is placed between the adherends, and pressure is applied by bagging the assembly and placing it under vacuum [1]. Electrical current is then passed through the prepreg, which creates heat at the bondline and cures the adhesive film. Since the method applies heat directly at the bondline and does not aim to heat the entire structure, it is more efficient when compared to heating from the outside (e.g., using a heat blanket) or heating the entire structure (in an autoclave). Moreover, since the heat is applied at the bondline, the temperature on the outside of the bondline does not have to be higher than that at the bondline (e.g., as with an external heat blanket), which reduces the potential for damage of temperature sensitive components that might already be attached to the adherends [11]. Additionally, the carbon fiber heater is the same material as the CFRP adherends, and it

does not require additives in the adhesive, e.g., as needed with inductive heating, which may compromise the delamination toughness and lead to certification issues [1]. Finally, embedded heaters provide uniform bond temperatures at the bondline. Thus, the embedded heater approach can be used both for manufacturing large composite structures and also to bond repair plugs to composite structures, which can increase the sustainability of large composite structures such as wind turbines and airplanes [1].

The embedded heater approach for adhesive bonding of composites provides a localized heating method at the bondline. Nevertheless, a concern is whether there is a loss in delamination toughness when using this embedded heater approach that may be due to more voids in the bond or some other unforeseen issue. The main contribution of this work is the comparative evaluation of the delamination toughness, $G_c$, of parts produced with the embedded heater method to that of parts bonded in an autoclave. Previous studies have shown that embedded heater bonded specimens offer similar bond strength under mode II loading [11]. However, a majority of actual fracture cases for metals are due to mode I loading [12]. Mode I tests are traditionally done by performing a double cantilevered beam test with unidirectional carbon fiber. However, the majority of applications do not use specimens of this type [13]. This being the case, the delamination toughness was evaluated under mode I dominated loading and a modified single cantilever beam test often used to evaluate delamination toughness in honeycomb structures [14]. Two different mode I dominated loading types were tested: quasi-static loading and fatigue loading.

Experimental results show that the delamination toughness of specimens joined using a carbon fiber embedded heater was comparable to samples joined in an autoclave for both quasi-static and fatigue loading conditions.

# SAMPLE DESIGN AND BONDING

## Adherend fabrication

The sample was designed to mimic the joining of a stringer to the skin of an aircraft wing as in Fig. 1, which allows the evaluation of the delamination toughness by peeling the skin from the stringer.

The C-channel (that mimics an aircraft stringer, as shown in Fig. 1) and skin were both fabricated with carbon/epoxy woven prepreg (Cycom 970). The C-channels were stacked in a $[45,0]_s$ and the skins in a $[45,0,45,0]_s$ quasi-isotropic stacking sequence and cured in an autoclave at 177°C for 120 minutes with a ramp rate of 2°C/min and a 586 kPa overpressure as recommended by the manufacturer Hexcel.

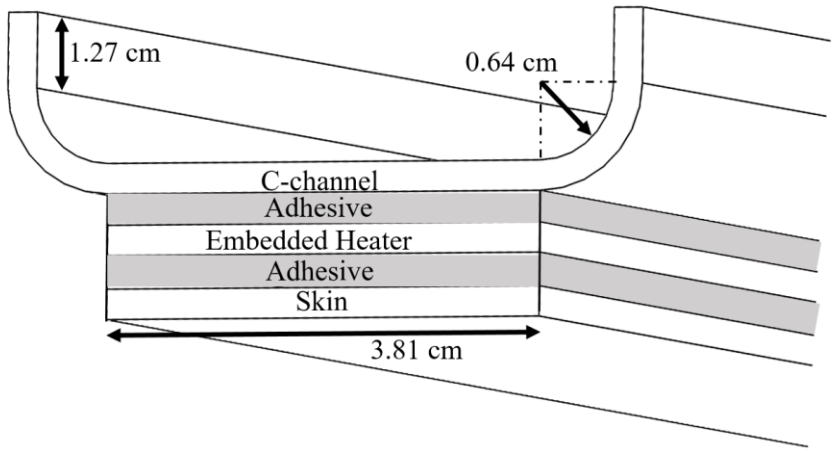


**Fig. 1.** A cross-sectioned view of the C-channel, thin film adhesive, embedded heater, and skin. Note that the thickness of each layer is not to scale.

The woven-prepreg samples were created in batches of ten. The prepreg was cut so the C-channel pieces would be 10.16 cm x 53.34 cm and the skins 3.81 cm x 53.34 cm. The skins were sized to be the same length and width as the flat surface of the C-channels. To create the C-

channels, the prepreg was then draped over an aluminum mandrel (shown in Fig. 2), which was 5.08 cm in width and height with 0.64 cm rounded edges, 0.7 m long, and was covered with nonpermeable release film. The skins were laid out on a steel caul plate and bagged separately. After the samples were cured the C-channels were cut to have 1.27 cm long flanges and be 25.4 cm in length. The skins were created individually to be 25.4 cm long and 3.81 cm wide.

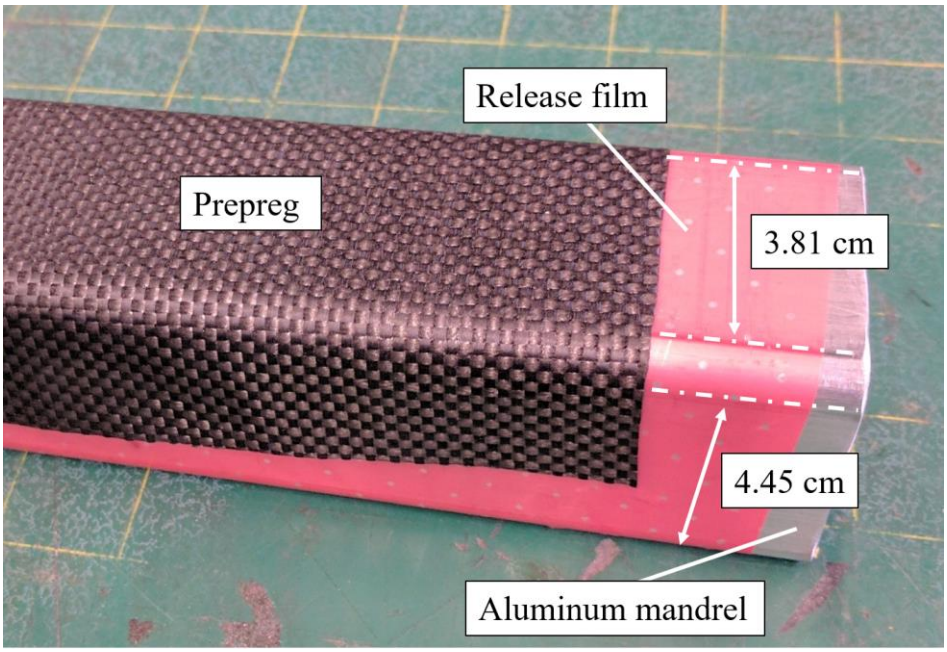


**Fig. 2.** Prepreg was draped over an aluminum mandrel to create the C-channels.

## Bonding

The samples were bonded using two methods: in an autoclave and utilizing an embedded heater. During embedded heater bonding, a single layer of a different carbon/epoxy woven prepreg (HCS2402-015-05) was used as the embedded heater instead of the same material that the adherends were constructed with. This new material cures at 127°C instead of 177°C, meaning that bonding can occur at a lower temperature. This is required to prevent the thin film adhesive from running, causing the adherends to come in contact with the embedded heater.

Before the adherends could be bonded, tests were performed without adhesive (referred to hereafter as a dry run) to ensure temperature uniformity and to find the control temperature [1]. Fig. 3 summarizes the procedure used to bond the adherends. First, insulation was placed over a rubber caul plate, and then a layer of Teflon was added (Fig. 3a). The skin was added, on which five type K thermocouples were taped, evenly spaced (Fig. 5b), to the surface of the skin on the side facing the caul plate. These are the outer thermocouples that are used later to control the temperature at the bondline during bonding. A layer of Kapton tape was placed between the thermocouple bead and the surface of the skin to electrically insulate the thermocouple. Teflon covered copper plates were positioned below the copper strips to act as heat sinks (Fig. 3b). A layer of Teflon was then placed over the skin to simulate the adhesive. Two layers of copper tape were applied to the ends of the embedded heater and then clamped to ensure full contact with the prepreg. The embedded heater was placed over the skin. Another layer of Teflon was added to simulate the second layer of adhesive. Five more bondline thermocouples were taped to the surface of the C-channel to measure the temperature at the bondline during dry runs with the Teflon layers and without the adhesives (Fig. 5b). The C-channel was placed directly over the skin (Fig. 3c). A Teflon coated aluminum stiffener was added to support the adherends to ensure the uniform bond pressure needed to keep the adherends from pressing through the adhesive during later tests (Fig. 3d). This may only be needed for thin adherends. Terminals were attached to the copper strips so that current could be passed through the embedded heater. A layer of Teflon was then added (Fig. 3e). Several layers of bleeder fabric (to act as insulation) and a layer of bagging film were added and the air removed (Fig. 3f). The sample was heated to 127°C for one hour with a ramp rate of 2°C/min as per the manufacturer's specifications. Fig. 4 shows the end view of the layup.

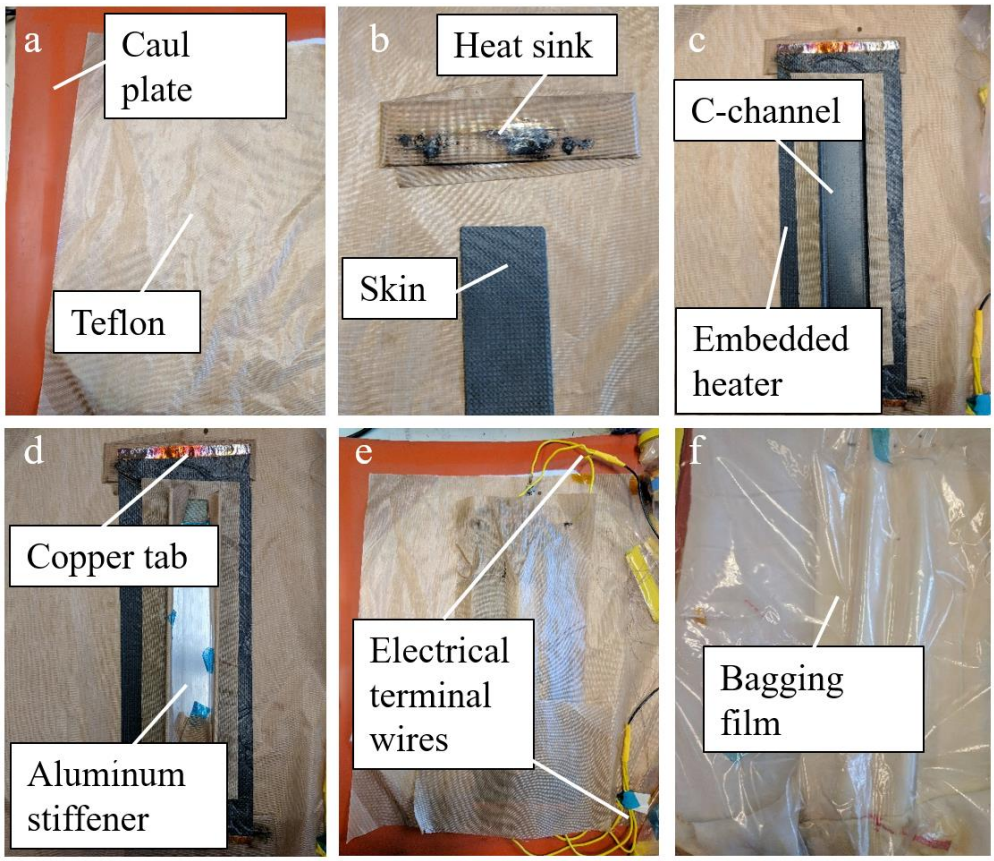


**Fig. 3.** Steps used to bond the adherends. (a) Rubber caul plate with added insulation and Teflon. (b) Added skin and Teflon wrapped copper heat sink. (c) Added Teflon in place of adhesive (during the dry run), embedded heater, Teflon, and then C-channel. (d) Added aluminum stiffener. (e) Attached copper terminals and added a layer of Teflon. (f) Added bleeder fabric and bagging film and then placed under vacuum.

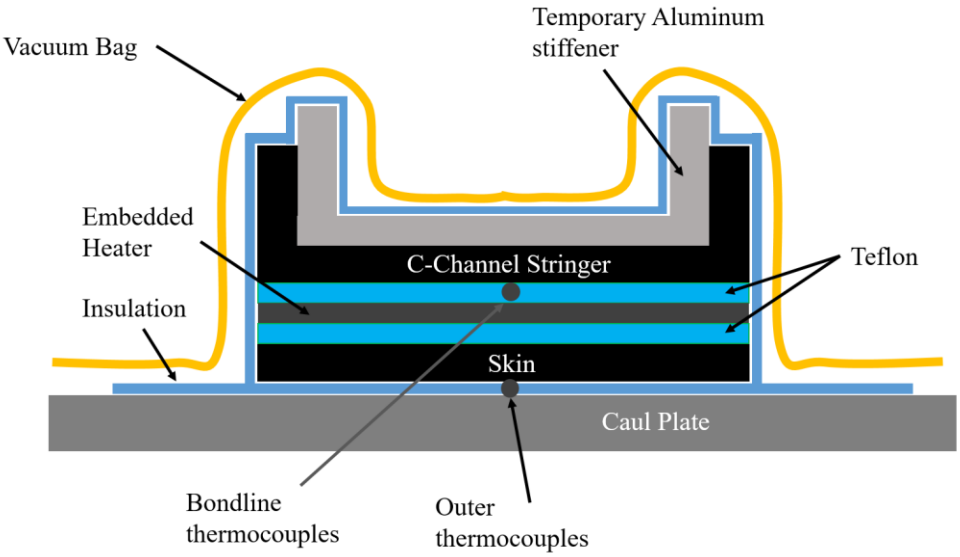


**Fig. 4.** End view of the bagged sample.

Multiple ways of bonding the C-channel and skin using an embedded heater were attempted. At first ten thermocouples were evenly placed along the part at the bond (Fig. 5a). Tests showed that the temperature was uniform across the width of the sample and only five thermocouples were required along the length in the center, Fig. 5b.

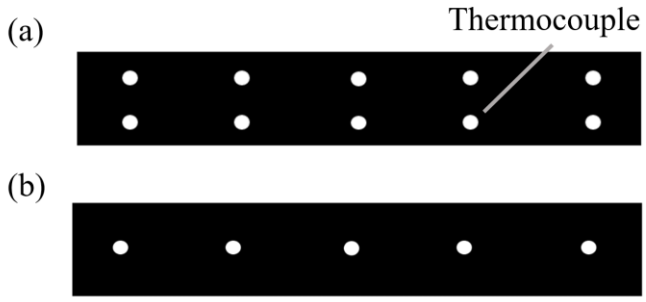


**Fig. 5.** Top view of the bond area showing the positions of the five thermocouples at the bondline. (a) Initial thermocouple locations. (b) Final thermocouple locations. The five thermocouples outside of the bondline are similarly positioned

Multiple heater sizes were tested. Electrical current was applied in two different directions (Fig. 6a and Fig. 6b). First electrical current was passed across the width of the bond (Fig. 6a), however the temperature ranged by 15°C. Passing the electrical current along the length of the bond (Fig. 6b), lowered the range by 32% to 10.4°C. However, these temperatures were still not constant enough. It was found that when the heaters were too narrow; edge affects caused nonuniform temperatures (Fig. 6a and Fig. 6b). This may be in part due to heat loss at the edge of the heater. To compensate for this extra material was added to achieve uniform temperatures at the bond (Fig. 6c), where the range in temperatures was only 3.9°C. The final heater configuration is shown in Fig. 7.

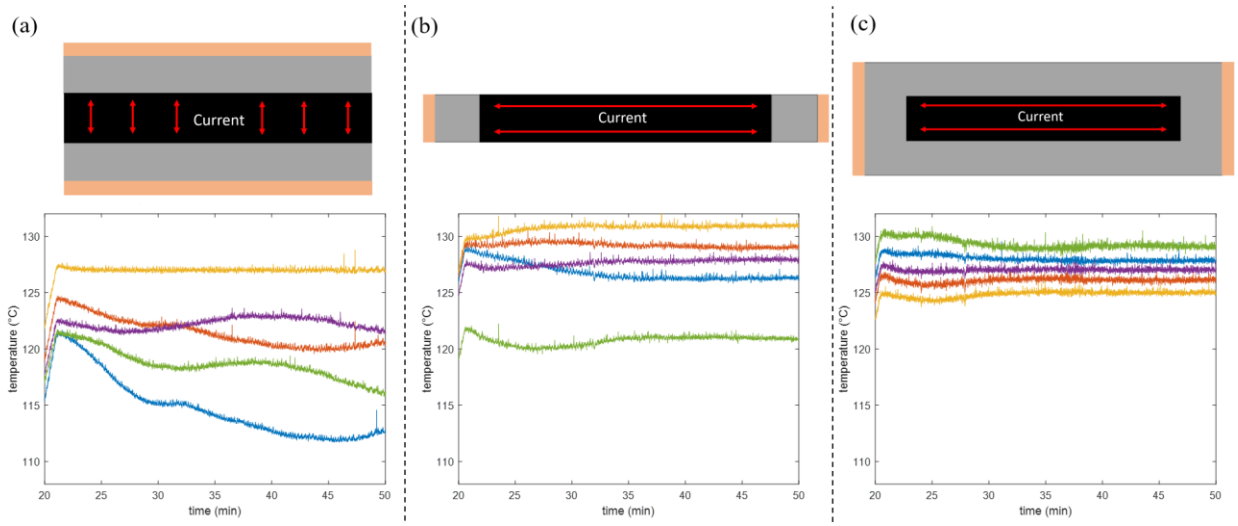


**Fig. 6.** The design evolution of the embedded heater. (a) Temperatures recorded at the bondline when current was passed along the width of the part. (b) Temperatures recorded at the bondline when current was passed along the length of the part. (c) Temperatures recorded at the bondline for the final heater configuration.

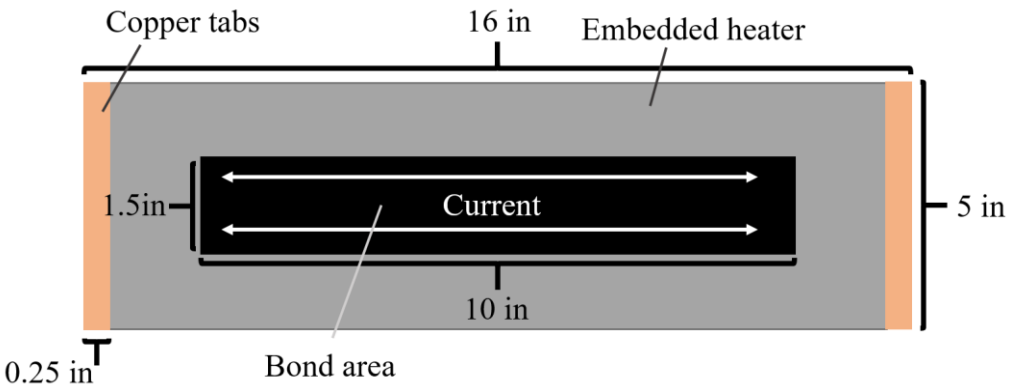


**Fig. 7.** Final heater dimensions with added material to avoid edge effects. The black section marks the bond area.

A temperature controller was used to regulate the bondline temperature with the embedded heater during actual bonding. However, a problem is that sensors placed at the bondline to control the temperature could lead to loss of delamination toughness. Therefore, the outer thermocouples placed outside of the skin (as in Fig. 4) were used to control the temperature. Since the temperatures outside are expected to be lower than the bondline, the reduction in the temperature was estimated experimentally for the specific test sample. First, a test was performed with the adhesives replaced with Teflon sheets as in Fig. 4 (a dry run where the adherends are not bonded) with five thermocouples placed at both the bondline and on the outside of the skin. The average of the five thermocouples at the bondline were used to maintain the bondline temperature to be 127°C (Fig. 8a) and the average temperature $T_{out}$ at the outer thermocouples were measured as $T_{out}$ =125°C. Next, the average temperatures of the five thermocouples above the skin (outside the bondline) was used as the new control temperature ($T_{out}$ =125°C) during a second dry run to verify that bondline temperatures were close to 127°C as seen in Fig. 8b, which compares the bondline temperatures for both dry runs. The Teflon sheets were replaced with thin film adhesive (Scotch-Weld AF 163-2K) and the bondline

thermocouples removed during actual bonding [11]. The excess embedded heater was trimmed away after curing.

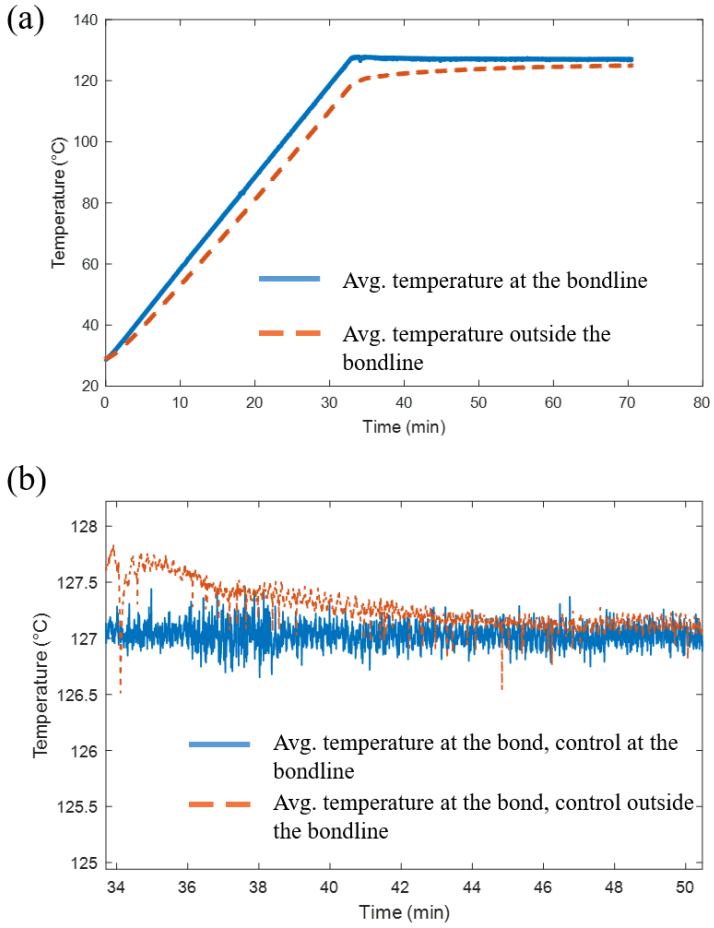


**Fig. 8.** Similarity of achieved bondline temperature when using (i) outer thermocouples (outside the bondline) and (ii) inner thermocouples (at the bondline) for temperature-control feedback. (a) Plot of the first dry run used to determine the control temperature $T_{out}$ at the outer thermocouples. The average of the five thermocouples at the bondline was used to control the bondline temperature at 127°C. (b) Plot of the average bondline temperatures for (i) the first dry run with feedback from the thermocouples at the bondline and (ii) the second dry run with feedback from the thermocouples outside of the bondline to control the outer temperature at $T_{out}$.

The autoclave samples were bagged using the same method as the embedded heater samples. However, the embedded heater was pre-cut to be the same size as the bond area so it did not have to be trimmed later. The same ramp rate, cure temperature, and cure time was used, though a 586 kPa overpressure was also applied. The temperature was monitored using an air temperature thermocouple as it was deemed that the parts were too thin to require bondline thermocouples.

# CHAPTER 2

## QUASI-STATIC TESTS

### Experimental setup

The delamination toughness was evaluated using a single-cantilevered beam test often used to evaluate toughness in composite honeycomb structures [14]. The stringer, in the shape of a C-channel, was placed with the flanges facing downward. The stringer was clamped from the sides with an aluminum support in the middle to ensure no deformation of the specimen (Fig. 9b). A 5 cm wide piece of Teflon tape was used to initiate the crack. The Teflon was placed between the embedded heater and the skin (Fig. 9). An aluminum block was adhered to the skin so that a hinged load $P$ could be applied to peel the skin off the fixed C-Channel. The load was applied at 30 mm/min until the crack length $a$ (in Fig. 9a) was propagated approximately ten millimeters from the edge of the Teflon tape and then the system was unloaded at 30 mm/min until it reached a zero load. The actual crack length was recorded for use later. The crack length was monitored using two cameras, one on each side of the specimen. The load $P$ and the load point displacement $\delta$ were recorded continuously at 10 Hz. The process was replicated five more times, for a total of six load cycles. Each time the crack was extended approximately 10 mm.

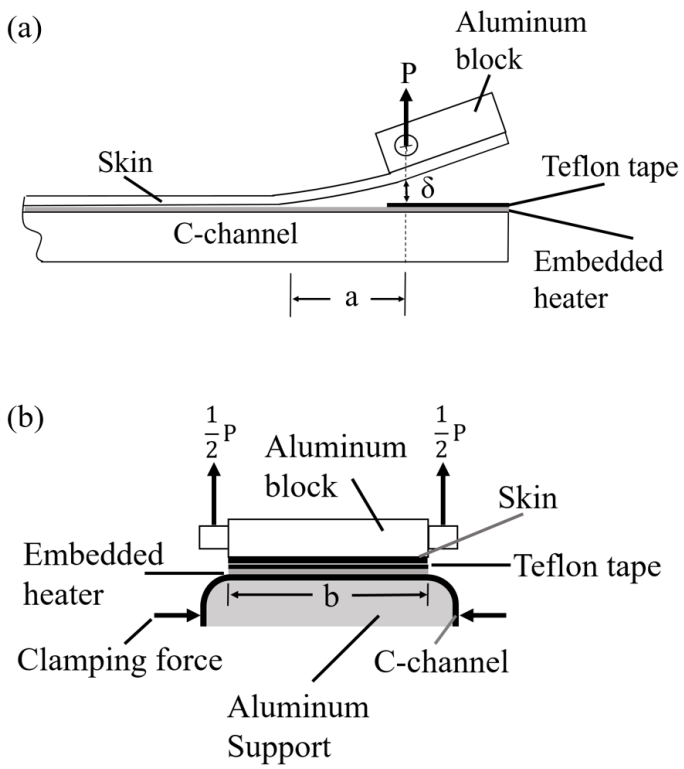


**Fig. 9.** Quasi-static peel test. (a) Side view. (b) End view.

*Areas method*

The critical delamination toughness $G_c$ was calculated using the areas method [15], as

$$G_c = -\frac{\partial(U)}{\partial A} = -\frac{1}{b}\frac{dU}{da} \qquad (1)$$

In the above $G_c$ is the critical delamination toughness, $A$ is the bond area exposed by the force used to open the crack, $U$ is the potential energy of the system, $b$ is the average width of the bond area and $a$ is the crack length (Fig. 9a). To compute $dU$ the pulling force $P$ was plotted against the load point displacement $\delta$ as shown in Fig. 10. The area in each load cycle curve, $dU$, was computed numerically.

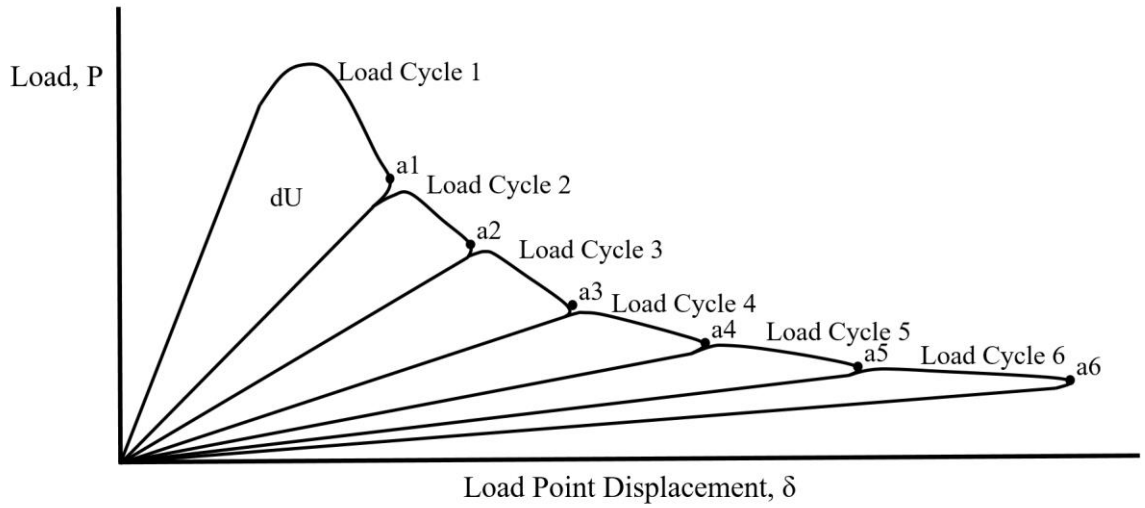


**Fig. 10.** Load displacement responses for six load cycles. The energy dissipated per load cycle, *dU*, was determined for all six load cycles to determine six values of delamination toughness.

Six load cycles were performed, yielding six values of $G_c$. The first value can be discarded since the crack was started artificially.

## Experimental results

The delamination toughness was evaluated with the quasi-static peel test using five samples for each bonding method. In some samples the crack jumped to a neighboring interface, a common issue seen in other studies [16][17].

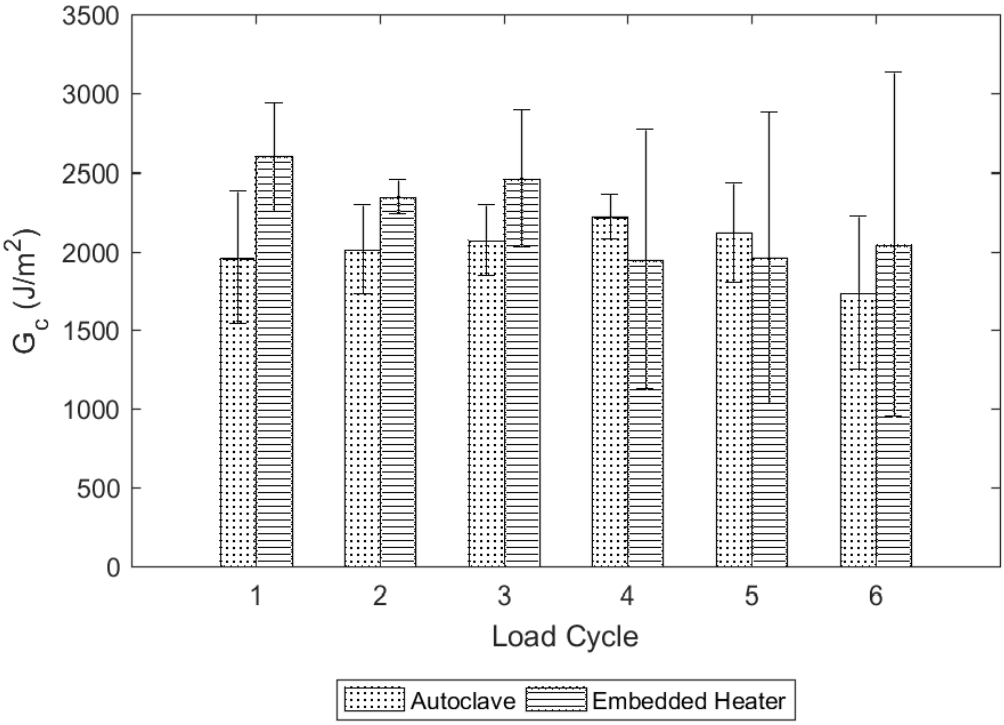


**Fig. 11.** Comparison of the mean (over five samples) delamination toughness for both bonding methods with the error bounds referring to one standard deviation.

As seen in Fig. 11, the delamination toughness was constant within a standard deviation for each load cycle which is consistent with other studies using woven fabric [18]. Both bonding methods have similar values for delamination toughness for load cycles two through six. The first load cycle can be discarded since the crack was started artificially. The larger standard deviations for the embedded heater samples may be because they were bagged and bonded individually while the autoclave samples were bonded all at the same time in the same bag. Table 1 shows that the observed mean delamination toughness for both bonding methods are comparable.

**Table 1** Comparison of the mean delamination toughness calculated from load cycles two through six for each sample.

| | Delamination Toughness ($J/m^2$) | |
|---|---|---|
| Sample | Autoclave | Embedded Heater |
| 1 | 2178 | 1440 |
| 2 | 1882 | 2637 |
| 3 | 2120 | 1714 |
| 4 | 1985 | 2268 |
| 5 | 2003 | 2702 |
| Mean | 2034 | 2152 |
| STD | 117 | 559 |

# CHAPTER 3

## METHODS FOR CALCULATING DELAMINATION TOUGHNESS

During the quasi-static tests the areas method was used to determine delamination toughness. Unfortunately, it requires that many points be taken during a load cycle to determine *dU* numerically. This is not possible during fatigue testing as the crack growth is too small to measure for each load cycle to accurately determine. To remedy this issue other methods of calculating delamination toughness were used. Three alternative methods were tested.

### Modified beam theory

Modified beam theory (MBT) is a common method used to determine delamination toughness. This method elaborates on the definition of delamination toughness using the potential energy of a linearly elastic system [19].

$$U = \frac{1}{2}\int_v \sigma_{ij}\varepsilon_{ij}dv - \int_0^\delta P(\delta)d\delta \qquad (2)$$

Here, $U$ is the potential energy, $\sigma_{ij}$ the stress, $\varepsilon_{ij}$ the strain, and $v$ the volume. The first term represents the energy stored in a linear elastic body while the second term is the work produced by the load $P$. The first term can be expressed as the force acting on the system.

$$U = \frac{1}{2}P\delta - \int_0^\delta P(\delta)d\delta \qquad (3)$$

Equations (1) and (3) can be combined to form

$$G = -\frac{1}{2b}\frac{\partial P}{\partial a}\delta - \frac{1}{2b}P\frac{\partial \delta}{\partial a} + \frac{1}{b}P\frac{\partial \delta}{\partial a} = \frac{1}{2b}\left(P\frac{\partial \delta}{\partial a} - \delta\frac{\partial P}{\partial a}\right) \qquad (4)$$

which can be simplified to

$$G = \frac{P^2}{2b}\frac{dC}{da} \qquad (5)$$

where C is the compliance. The compliance can be defined as shown [19].

$$C = \frac{\delta}{P} = m(a + \Delta)^3 \qquad (6)$$

In Eq. (6) *m* is a constant and a correction factor *Δ*. This correction factor is required to compensate for the fact that at the "fixed" end of the cantilever (i.e., at the crack tip) the slope and the deflection are not zero [20]. Factor *Δ* is found by plotting the cube of the compliance against the debond length (Fig. 12).

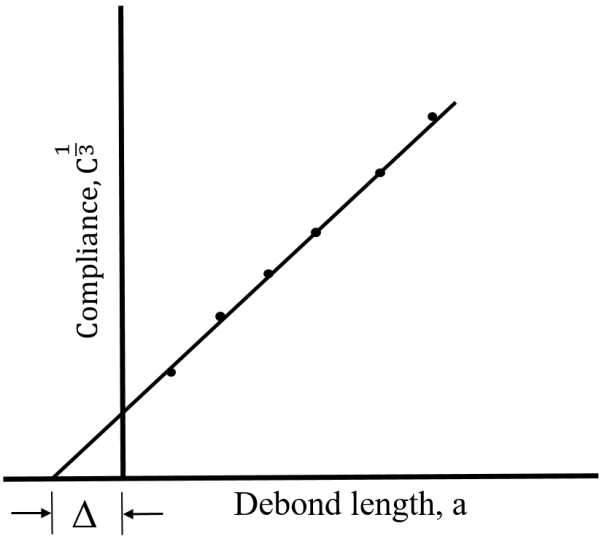


**Fig. 12.** Plot of the debond length and the cube of the compliance to determine *Δ*.

The relation shown in Eq. (6) is common for the double cantilevered beam method and can be substituted into Eq. (5) to get Eq. (7).

$$G = \frac{3P_{max}\delta_{max}}{2b(a+|\Delta|_{avg})} \qquad (7)$$

In Eq. (7) $P_{max}$ is the force at the maximum displacement $\delta_{max}$. A linear beam is assumed in the formulation, which may cause errors at large load point displacements. In addition, the formula does not consider shear stress which no longer becomes negligible at large load point displacements.

Areas compliance method

While modified beam theory has been used by other researchers extensively, it assumes a linear beam. The high deflection observed during the quasi-static tests caused the specimen to violate the small angle approximation that could then result in inaccurate values for delamination toughness. The areas compliance method (AC-method) was created to help remedy this issue.

The AC-method relies on the areas method in its formulation. First, the delamination toughness was calculated for each load cycle using the areas method. Then Eq. (5) was rearranged.

$$\frac{dC}{da} = \frac{Gb}{P^2 a} \qquad (8)$$

The delamination toughness $G$ was calculated using the areas method. The relation $\frac{dC}{da}$ was computed for every load cycle for each sample and plotted against the crack length, $a$.

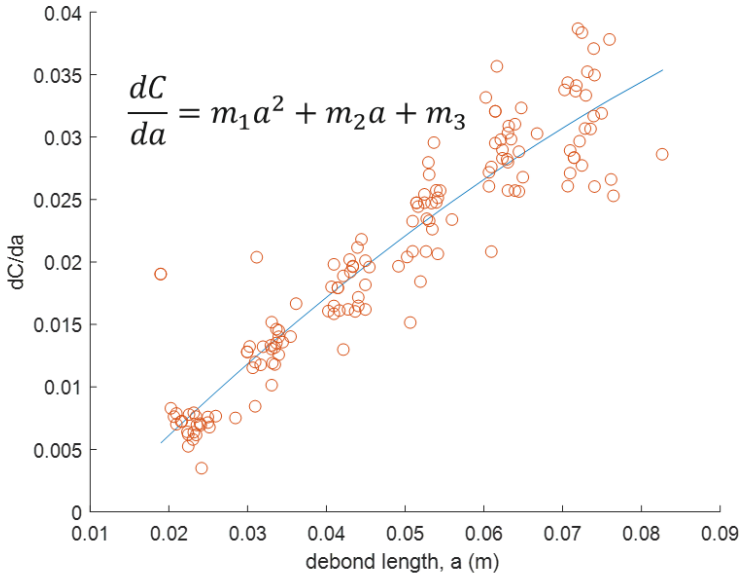


**Fig. 13.** Plot showing $\frac{dC}{da}$ plotted for each value of *a*.

$$\frac{dC}{da} = m_1a^2 + m_2a + m_3 \qquad (9)$$

A second order polynomial was fit to the scatter plot so that $\frac{dC}{da}$ could be found at every value of *a*. This relation was then substituted into Eq. (5) to find the delamination toughness.

$$G = \frac{P^2}{2b}\frac{dC}{da} = \frac{P^2a}{2b}(m_1a^2 + m_2a + m_3) \qquad (10)$$

Compliance curve method

The CA-method requires that the areas method first be used to determine delamination toughness and then a relation for $\frac{dC}{da}$ found. Since it is not clear whether the areas method is providing accurate results a new method of calculating delamination toughness is required. Instead of finding the relation between compliance and debond length *a* via the areas method, this new method, dubbed the compliance curve method (CC-method), finds the relation directly

through experimentation. First, the compliance *C* was computed for each loading cycle using the force *P* at the maximum load point displacement and that load point displacement. Then the compliance was plotted against the final crack length for each loading cycle. All test samples were plotted on the same graph to determine a second order polynomial with coefficients $m_1$, $m_2$, and $m_3$ that best describes the compliance verses crack length relation. To produce a better curve fit a weighted number of points was placed at the origin since the load and therefore the compliance is zero at a crack length of zero.

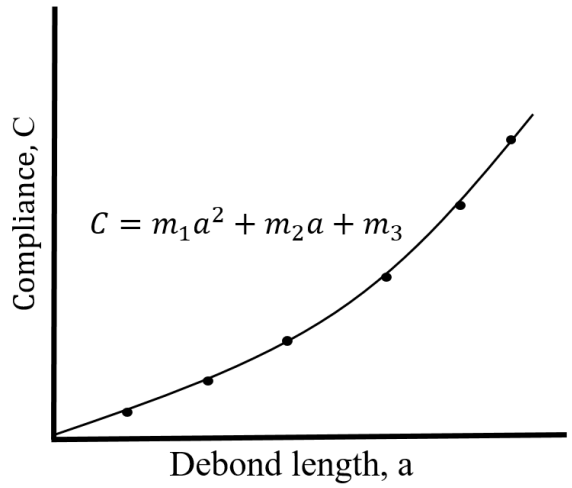


**Fig. 14.** Compliance curve fit to compute *G*.

A derivative was taken of the polynomial and substituted into Eq. (5) to compute *G* as shown below.

$$G = \frac{P^2}{2b}\frac{dC}{da} = \frac{P^2}{2b}(2m_1a + m_2) \qquad (11)$$

Comparing methods for determining delamination toughness

All four methods (areas method, modified beam theory, the areas compliance method, and the compliance curve method) were calculated for the quasi-static tests to determine which is

the most consistent for the last five load cycles. Fig. 15 compares all the methods for the five samples bonded in an autoclave and using an embedded heater.

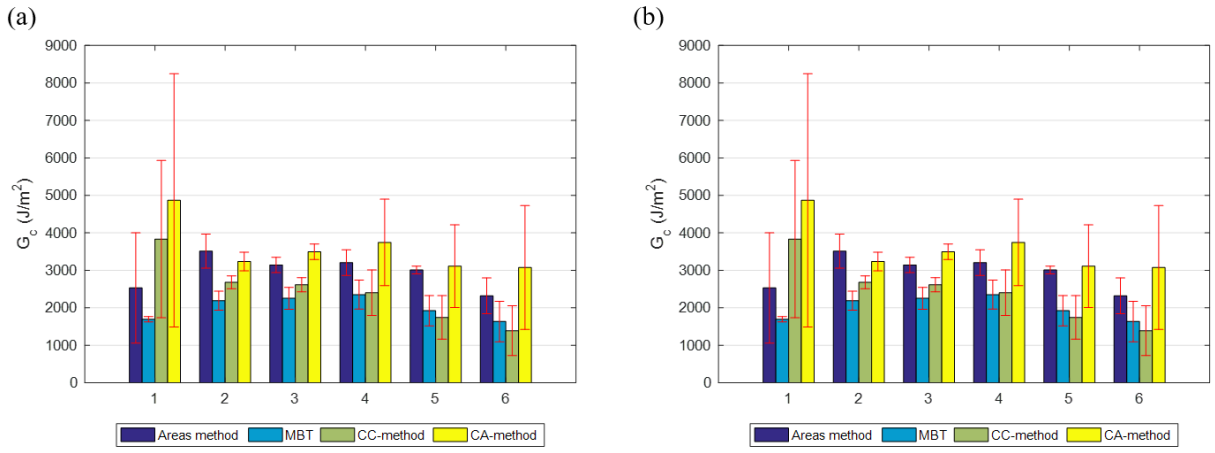


**Fig. 15.** Comparison of the mean (over five samples) delamination toughness calculated four ways for the C-channel samples. The error bounds refer to one standard deviation. (a) Five samples bonded in an autoclave. (b) Five samples, each bonded using an embedded heater.

As seen in the figure the areas method and CA-method provides the most consistent results. MBT and the CC-method both under predict.

The results from the quasi static tests have a great deal of noise due to the low sample size. To determine which method is the most consistent a larger sample size is needed. It was beyond the scope of this paper to create more samples so data was used from a round robin study that performed the same quasi-static tests for the sandwich composite samples pictured in Fig. 16. Fig. 17 shows a comparison of the methods for 25 sandwich composite samples.

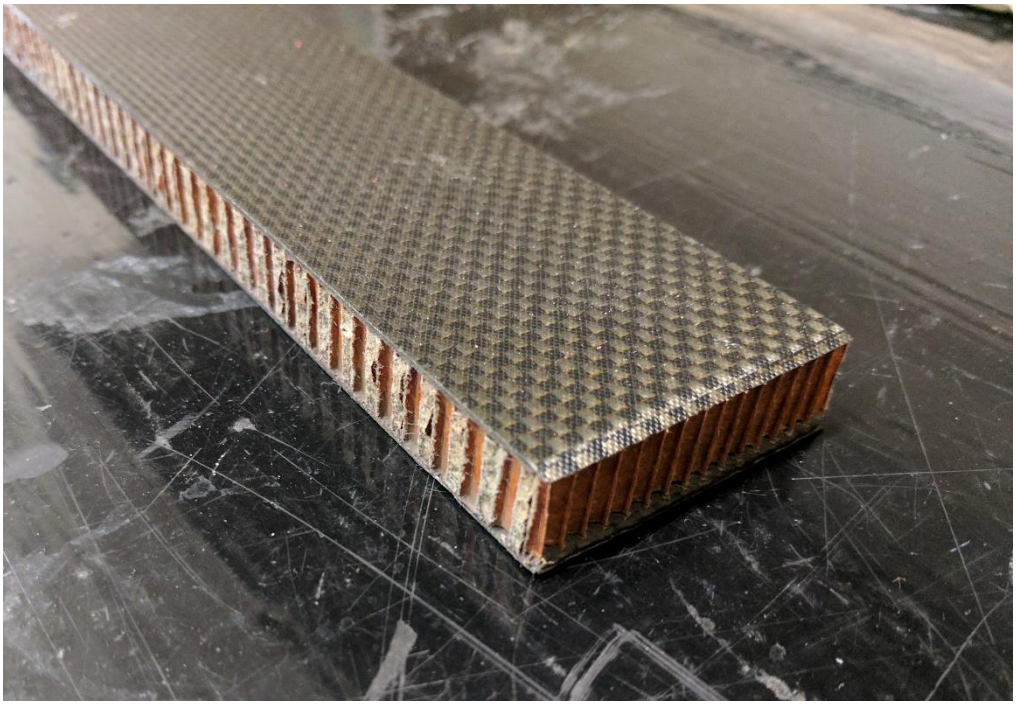

**Fig. 16.** An example of a sandwich composite sample.

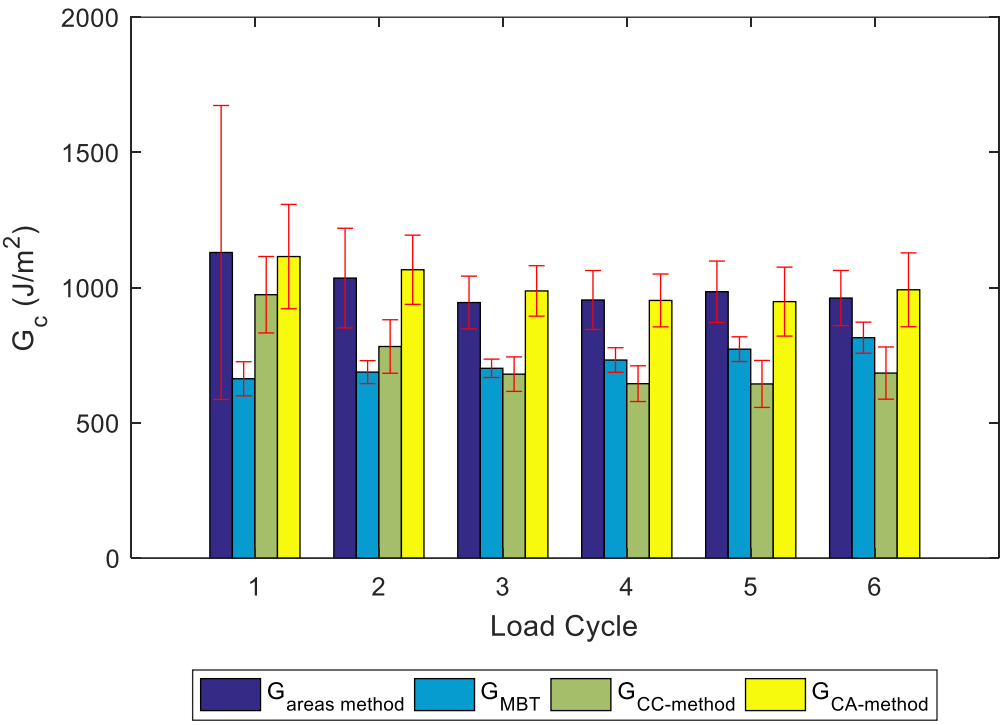


**Fig. 17.** Comparison of the mean (over 25 samples) delamination toughness calculated four ways for the sandwich composite samples. The error bounds refer to one standard deviation.

The data here is much clearer showing that the areas method is the most constant with each load cycle. Modified beam theory rises steadily and therefore cannot be used during fatigue testing. Of the last two methods, the CC-method, while less constant than the CA-method, should be used for fatigue testing as it is somewhat constant and does not rely on the areas method. The areas method cannot be utilized at all as it requires a numerical integration of the loading curve and the determination of the crack length for each load cycle, both of which are near impossible to calculate during fatigue testing.

# CHAPTER 4

## FATIGUE

It is useful to know the delamination toughness not only for quasi-static loading, but also for fatigue loading. Furthermore, fatigue testing is very important as it allows users to predict crack growth for a joint undergoing fatigue loading. This can prove invaluable in fields such as the aerospace industry where the simple act of measuring the length of a crack can help determine the remaining life cycle of the joint before catastrophic failure. While measuring crack growth under quasi-static loading for composites is relatively well explored, there is no standard for fatigue loading [21]. In fact, there is no consensus on the similitude parameter used to interpret experimental data, making comparisons outside of a single study difficult [22]. This being the case, fatigue testing was performed using the same samples as used in the quasi-static tests under custom testing conditions.

### Experimental setup

Fatigue testing was performed similarly to the ASTM standard D6115 [23] for double cantilevered beams. The setup was the same as with the quasi-static peel tests using a Instron 8511.

First, a load was applied until the crack propagated from the edge of the Teflon tape (approximately 20 mm) to near 27 mm. This was done so fatigue testing could begin with a natural crack. From there the machine was unloaded to a force below that of the quasi-static tests ranging from 185 N to 270 N. The load point displacement was then oscillated at 2 Hz keeping a constant minimum and maximum force for a tension-tension load controlled test. All samples had an R-ratio of 0.66.

Fatigue testing was performed twice. In the first round of tests the load black was mistakenly glued on backwards so that the load was applied at the other side of the load block. This caused the load block to act as a stiffener and may have altered the results. The maximum displacement, the force at that displacement, and the crack length were recorded throughout, but only five points were used up to just before full delamination. The number of cycle was determined by counting frames from the time lapse video. In the second set of tests the load block was adhered properly and the tests were run longer. Due to hardware issues only the cameras were used to record the maximum and minimum displacements, number of cycles, and crack length on a single side. The two cameras (one monitoring crack length and the other pointed at the display of the Instron machine) took a single photo every 20 minutes. A single data point was recorded after at least a 0.5 mm of crack growth.

The delamination toughness was calculated using the CC-method method and modified beam theory. The constants $m_1$ and $m_2$ from Eq. 11 were found from the quasi-static tests. The results for fatigue testing were compared by plotting the crack length per number of cycles against the difference in the delamination toughness, $\Delta G$, using log plots also called Paris Plots.

$$\Delta G = G_{max} - G_{min} \qquad (12)$$

The maximum delamination toughness ($G_{max}$) was calculated using the maximum force during a single cycle. The minimum delamination toughness ($G_{min}$) was calculated using the minimum force during that same cycle. An example Paris Plot is shown in Fig. 18.

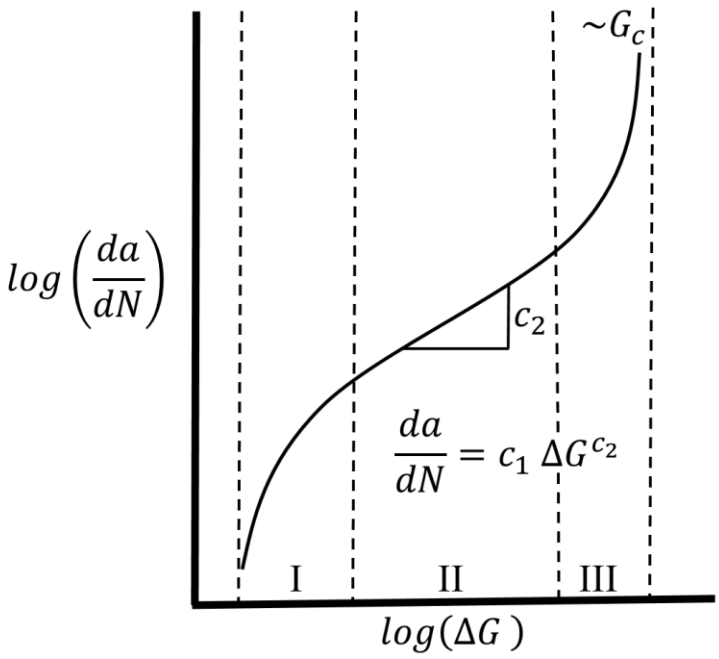


**Fig. 18.** An example Paris Plot. Paris's Law is fit as a power law to the middle region.

The Paris Plot can be separated into three regions. The section of interest is region II. Here a power equation, known as Paris's Law, is fit to the data to determine the relationship between crack length, number of cycles, and delamination toughness.

$$\frac{da}{dN} = c_1\,\Delta G^{c_2} \qquad (13)$$

The value *a* is the crack length and *N* the number of cycles. The constants $c_1$ and $c_2$ were determined from the fit.

## Experimental results

The quasi-static peel tests showed that the samples bonded using an embedded heater and those bonded in an autoclave had comparable bond strengths under a quasi-static load. Fatigue tests were performed to determine if this was also true for fatigue loading. Fig. 19 shows the

results from the first round of fatigue testing where the load block was adhered backward. Fig. 19a shows a plot comparing the two sample types with the delamination toughness computed using the compliance curve method.

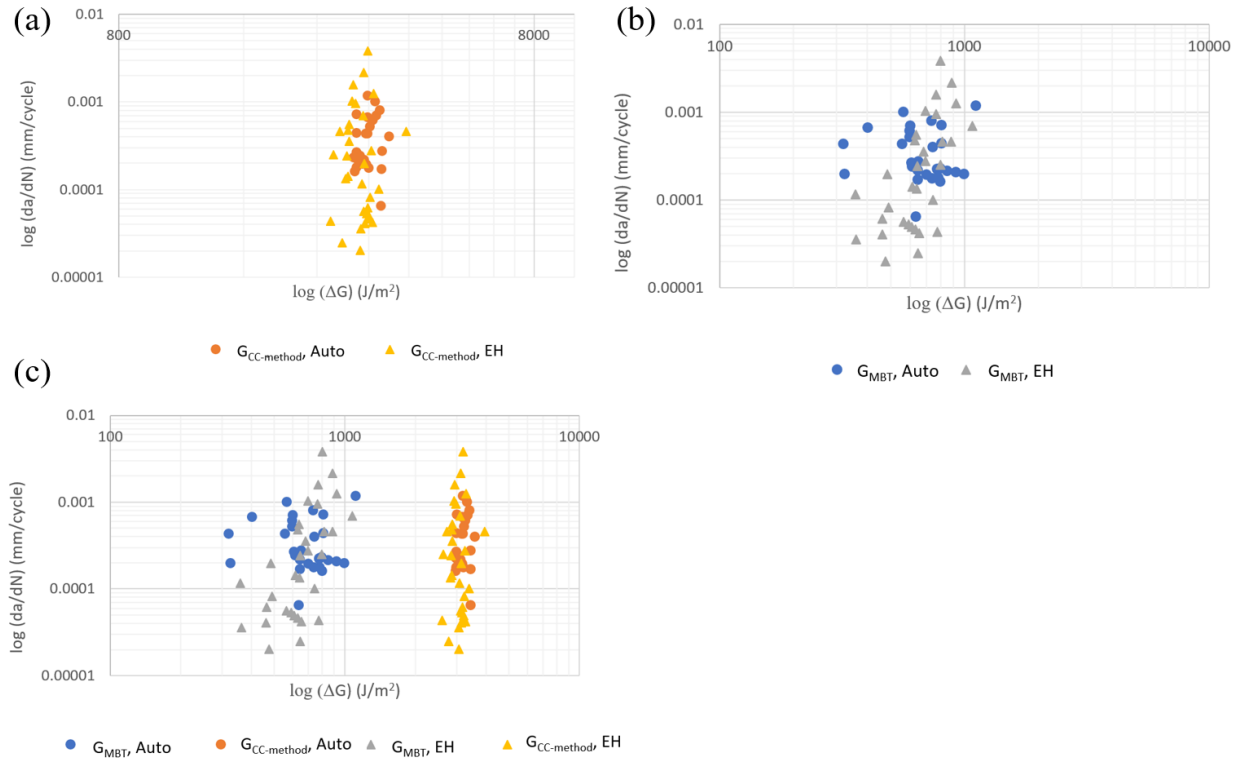


**Fig. 19.** Fatigue results from the first round of testing where the load block was improperly attached to the skin. Eight samples were tested for each bonding method. (a) A plot comparing the two bonding methods under fatigue loading. *G* was computed using the CC-method. (b) A plot comparing the two bonding methods under fatigue loading. *G* was computed using MBT. (c) A plot comparing the two bonding methods using MBT and the CC-method to calculate delamination toughness.

The figure shows that the bond strength under fatigue loading is approximately the same for both the autoclave bonded samples and those joined using an embedded heater. The same is true when delamination toughness was calculated using MBT (Fig. 19b).

Fig. 19c shows the difference between the two methods for both sample types. The figure shows that the delamination toughness is consistently high using the CC-method as opposed to MBT for both sample types. Unfortunately, the high degree of scatter in the results does not allow for the determination of a relation between crack length and delamination toughness using Eq. 13.

The second round of tests using the properly bonded load blocks produces very similar results. Fig. 20a compares both bonding methods using both modified beam theory and the CC-method to determine delamination toughness. There is an offset between the two calculation methods. However, the embedded heater bonded samples and the samples bonded in an autoclave have the same delamination toughness under fatigue loading conditions. Unfortunately, there is still too much scatter to fit Paris's Law. Fig. 20b shows the results from all the samples tested. The results from the first round of samples are in line with the results from the new samples. The steep slope of the data suggests that the data may correspond to region III of the Paris Plot seen in **Fig. *18***. In order to define regions I and II more fatigue tests at a lower mean load would be required. These tests would take a significant amount of time to perform and are beyond the scope of this study.

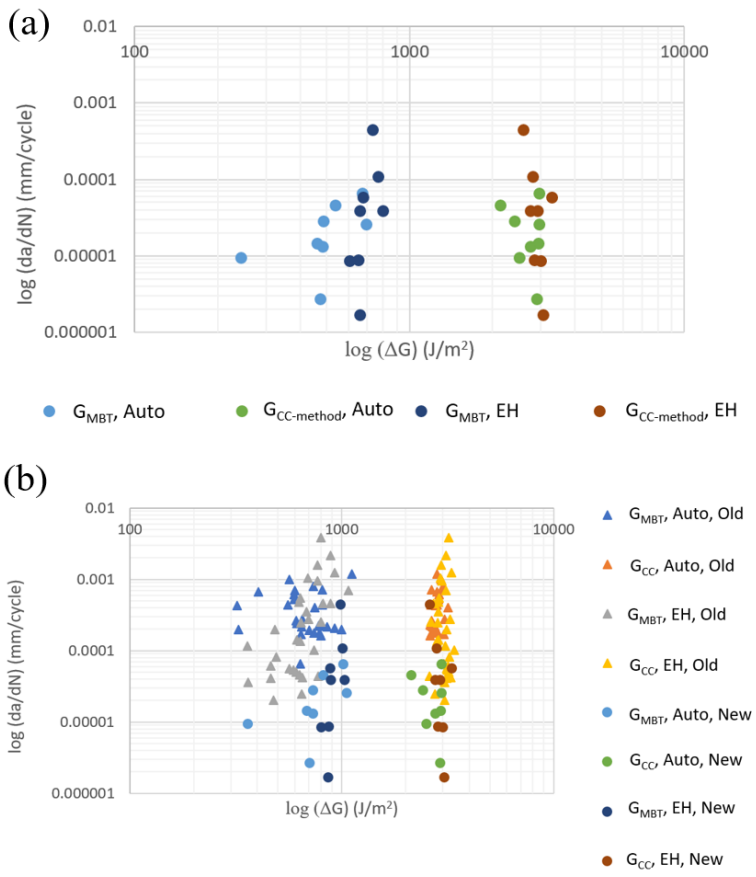


**Fig. 20.** Fatigue testing results. (a) Plot comparing the two bonding methods using MBT and the CC-method to calculate delamination toughness for the samples with the properly bonded load blocks. (b) Plot comparing the two bonding methods using MBT and the CC-method to calculate delamination toughness for all samples.

# CHAPTER 5

## CONCLUSION

### Discussion of results

Carbon fiber embedded heaters have great potential for use in manufacturing and repair. The results from the quasi-static peel tests show that under mode I dominated loading conditions adherends joined using embedded heaters have a similar delamination toughness as those bonded in an autoclave when delamination toughness is calculated using the areas method.

Under fatigue loading the data was far more scattered and did not allow for the determination of a relation between the number of cycles, delamination toughness, and the crack length. This may be because unidirectional prepreg was not used. Also, it was assumed that the captured data was in region II of the Paris plot. This may not necessarily be true. The steep angle of the results show that the data may have been in region III. This would further explain some of the discrepancies. However, the results still showed overlap for the two bonding methods. From this it can be concluded that the bond strength was comparable between the two bonding methods, showing that under fatigue loading they perform similarly.

### Future work

Future work for this testing method would require that unidirectional prepreg be used for the embedded heater and the skin. This may prevent the crack from jumping between layers and allow for a more precise knowledge of where the crack is and possible better results from the fatigue tests. In addition, a thicker skin could be used. This would allow for less deflection of the beam and less energy loss due to shear. This may result in modified beam theory being more accurate. If so then MBT may then be used to determine the accuracy of the new compliance

curve method during fatigue testing. In addition, a lower mean stress (preload) could be used to ensure that the tests run longer. This may produce data is in region II of the Paris Plot as desired. With these alterations, a relation for fatigue life could be determined.

# BIBLIOGRAPHY

[1] M. Ashrafi, S. Devasia, and M. E. Tuttle, “Resistive embedded heating for homogeneous curing of adhesively bonded joints,” *Int. J. Adhes. Adhes.*, vol. 57, pp. 34–39, 2015.

[2] P. K. Mallick, *Fiber-reinforced composites : materials, manufacturing, and design*, Third. CRC Press, 2008.

[3] K. S. Kim, J. S. Yoo, Y. M. Yi, and C. G. Kim, “Failure mode and strength of uni-directional composite single lap bonded joints with different bonding methods,” *Compos. Struct.*, vol. 72, no. 4, pp. 477–485, 2006.

[4] C. H. Wang, A. Rider, and J. Cao, “Internal resistance heating for homogeneous curing of adhesively bonded repairs,” *Mater. Forum*, vol. 34, no. 3, pp. 85–92, 2008.

[5] S. Turri, A. Sanguineti, and R. Lecchi, “Novel glass fiber-reinforced composites having a UV and peroxy curable fluoropolymer matrix,” *Macromol. Mater. Eng.*, vol. 288, no. 9, pp. 708–716, 2003.

[6] J.-H. Lu and J. P. Youngblood, “Adhesive bonding of carbon fiber reinforced composite using UV-curing epoxy resin,” *Compos. Part B Eng.*, vol. 82, pp. 221–225, 2015.

[7] T. J. Ahmed, D. Stavrov, H. E. N. Bersee, and a Beukers, “Induction welding of thermoplastic composites - An overview,” *Compos. Part a-Applied Sci. Manuf.*, vol. 37, no. 10, pp. 1638–1651, 2006.

[8] V. Tanrattanakul and D. Jaroendee, “Comparison between microwave and thermal curing of glass fiber-epoxy composites: Effect of microwave-heating cycle on mechanical properties,” *J. Appl. Polym. Sci.*, vol. 102, no. 2, pp. 1059–1070, 2006.

[9] C. Nightingale and R. J. Day, “Flexural and interlaminar shear strength properties of carbon fibre/epoxy composites cured thermally and with microwave radiation,” *Compos. - Part A Appl. Sci. Manuf.*, vol. 33, no. 7, pp. 1021–1030, 2002.

[10] H. S. Ku, “Contrast Joints of Glass-Fibre with Carbon-Fibre Reinforced Low Density Polyethylene Composite Bonded by Microwave Irradiation,” *J. Electromagn. Waves Appl.*, vol. 22, no. 1, pp. 69–84, 2008.

[11] B. P. Smith, M. Ashrafi, M. E. Tuttle, and S. Devasia, “Bondline Temperature Control for Joining Composites With an Embedded Heater,” *J. Manuf. Sci. Eng.*, vol. 138, no. 2, p. 21011, 2015.

[12] T. J. M.S. Sham Prasad, C.S. Venkatesha, “Experimental Methods of Determining Fracture Toughness of Fiber Reinforced Polymer Composites under Various Loading Conditions,” *J. Miner. Mater. Charact. Eng.*, vol. 10, no. 13, pp. 1263–1275, 2011.

[13] A. B. De Morais, “Double cantilever beam testing of multidirectional laminates,” *Compos. Part A Appl. Sci. Manuf.*, vol. 34, no. 12, pp. 1135–1142, 2003.

[14] R. K. Martin Rinker, James G. Ratcliffe, Daniel O. Adams, “Characterizing Facesheet/Core Disbonding in Honeycomb Core Sandwich Structure,” p. 39, 2013.

[15] a Standard, “D5528-01 2001. Standard Test Method for Mode I Interlaminar Fracture Toughness of Unidirectional Fiber-Reinforced Polymer Matrix Composites,” *Am. Soc. Test. Mater.*, no. Mode I, pp. 1–13, 2014.

[16] P. Robinson and D. Q. Song, “A Modified DCB Specimen for Mode I Testing of Multidirectional Laminates,” *J. Compos. Mater.*, vol. 26, no. ll, pp. 1554–1577, 1992.

[17] A. B. Pereira, A. B. De Morais, M. F. S. F. De Moura, and A. G. Magalhães, “Mode I interlaminar fracture of woven glass/epoxy multidirectional laminates,” *Compos. Part A Appl. Sci. Manuf.*, vol. 36, no. 8, pp. 1119–1127, 2005.

[18] M. Kotaki and H. Hamada, “Effect of interfacial properties and weave structure on mode I interlaminar fracture behaviour of glass satin woven fabric composites,” *Compos. Part A Appl. Sci. Manuf.*, vol. 28, no. 3, pp. 257–266, 1997.

[19] V. Tamuzs, S. Tarasovs, and U. Vilks, “Progressive delamination and fiber bridging modeling in double cantilever beam composite specimens,” *Eng. Fract. Mech.*, vol. 68, no. 5, pp. 513–525, 2001.

[20] J. G. W. Hashemi, S., A. J. Kinloch, “Corrections needed in double-cantilever beam tests for assessing the interlaminar failure of fibre-composites,” *J. Mater. Sci. Lett.*, vol. 8, pp. 125–129, 1989.

[21] L. Yao, R. C. Alderliesten, and R. Benedictus, “Interpreting the stress ratio effect on delamination growth in composite laminates using the concept of fatigue fracture toughness,” *Compos. Part A Appl. Sci. Manuf.*, vol. 78, pp. 135–142, 2015.

[22] L. Yao, Y. Sun, M. Zhao, R. C. Alderliesten, and R. Benedictus, “Stress ratio dependence of fibre bridging significance in mode I fatigue delamination growth of composite laminates,” *Compos. Part A Appl. Sci. Manuf.*, vol. 95, pp. 65–74, 2017.

[23] Astm D 6115-97, “Standard test method for mode {I} fatigue delamination growth onset of unidirectional fibre-reinforced polymer matrix composites,” *Am. Soc. Test. Mater.*, vol. 15.03, no. Reapproved, pp. 1–6, 2001.

# APPENDIX

## Determining face sheet thickness

Multiple dimensions were tested for the C-channel and skin. After some experimentation three face sheet (skin) layups were tested: $[45,0]_s$, $[[45,-45,0]_s$, and $[45,0,45,0]_s$. Two samples were cured for each layup, one with an added layer of prepreg to simulate the heater and one without. They were all bonded in a pressurized autoclave using the same curing specifications as the later finished samples. The four ply samples failed during the quasi-static tests and were discarded. Note that the crack was started between the C-channel and the prepreg for the parts that had the extra layer. Fig. A1 shows the load displacement response curves for the other samples.

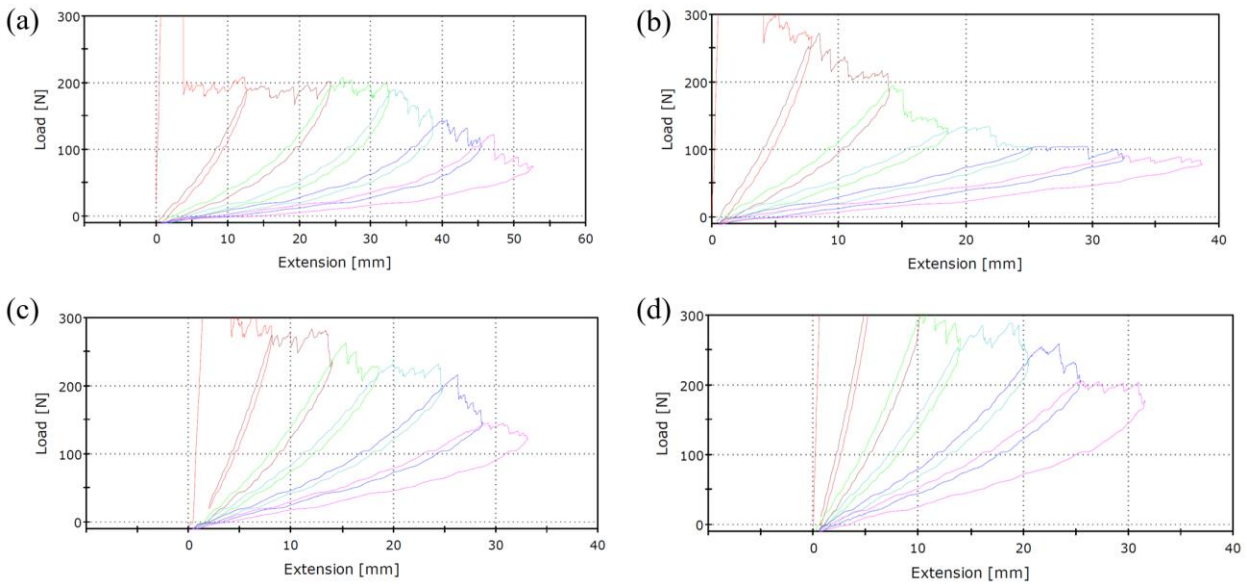


**Fig. A1.** (a) Six ply skin without an embedded heater. (b) Six ply skin with an embedded heater. (c) Eight ply skin without an embedded heater. (d) Eight ply skin with an embedded heater.

It was decided after these tests to use an eight-ply skin to prevent the skin from buckling. In addition, in later tests the crack was started between the skin and the embedded heater to ensure uniform skin thickness across all tests.

## Experimental issues

Several issues arose during the experiments. Some were corrected, while others will need to be addressed for future research.

- When bonding adherends using embedded heaters, the heater shorted, pressing through the electrically insulating adhesive and coming into contact with one of the adherends. This issue was corrected by adding an aluminum support inside of the C-channel, but could become a problem when bonding especially thin adherends or when a constant pressure cannot be easily applied across the bond area.
- There was some trouble generating enough power to get the embedded heater to the required temperature with some of the larger embedded heater designs. This was a limitation of the hardware and should be kept in mind for experiments that require a relatively large embedded heater.
- Insulating the thermocouples in Teflon tape kept them from shorting out on the carbon fiber and gave much more consistent temperature readings.
- A mistake was made with the initial tests where the load block was consistently glued on backwards. New tests were performed with the load block in the correct orientation and the original results discarded for the quasi-static tests.

Embedded heater standard operating procedure

**Purpose:**

Embedded heaters in the form of carbon fiber fabric can be used as a heating element when bonding two adherends (carbon fiber or otherwise) together, negating the need for an autoclave. The heater is placed between the two parts to be bonded with either Teflon sheets (during a 'dry run' when no bonding occurs) or an electrically insulating thin film adhesive (when actual bonding is needed) between it and the adherends. Current is passed through the heater to cause it to rise in temperature to cure the adhesive.

**Procedure:**

**1. Control system**

A custom system using two Arduino MEGA boards and other hardware was used to control the temperature of at the bondline when using an embedded heater. The system consists of seven main components: the main Arduino used to control the temperatures at the bond, relays to control the power output to the embedded heater, an Arduino MEGA slave board used to control the relays, a power supply for the embedded heater, two multiplexer boards, and a computer to monitor it all (Fig. A2).

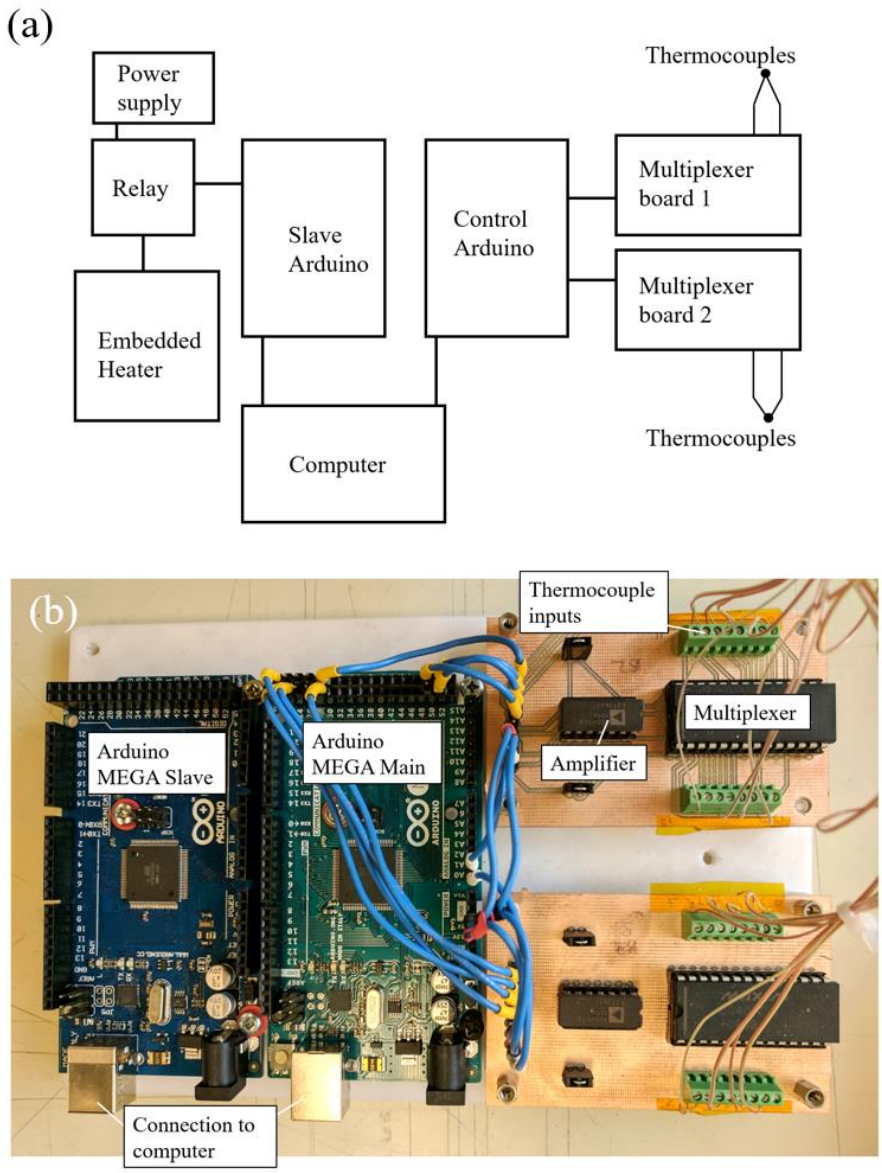


**Fig. A2.** (a) A box diagram of the control system. (b) A photo of most of the components.

Thermocouples used to control the bondline temperatures are connected to the Multiplexer boards which amplify the signal to be read by the main Arduino control board. Fig. A3 shows a circuit diagram of the multiplexer boards which contain a multiplexer so multiple thermocouples can be connected to a single analog input port on the Arduino and a thermocouple

amplifier which amplifies the voltage created by a thermocouple so that the Arduino can read it. The current system is designed to be used with type K thermocouples.

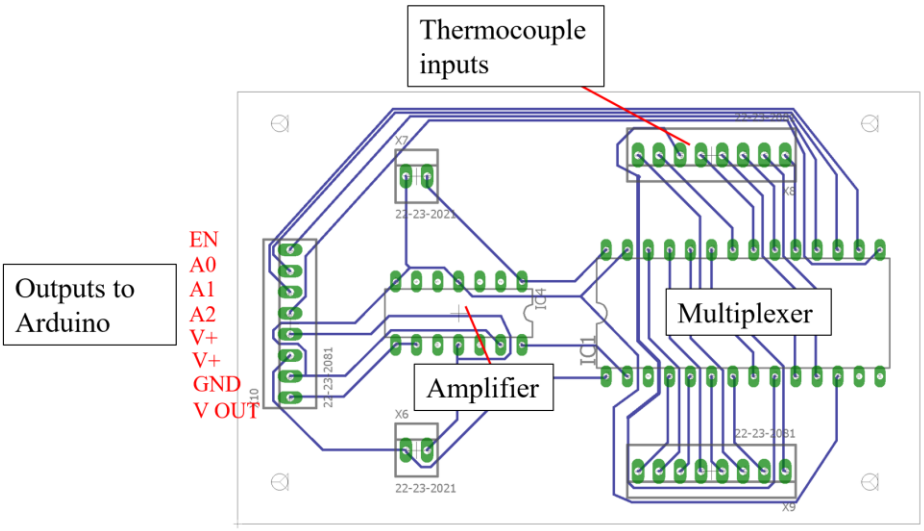


**Fig. A3.** A circuit diagram of a single multiplexer board.

Only a single relay is required to control one zone. For multizone support two relays are needed for each zone. Fig. A4 shows six of the twelve relays required to control six zones.

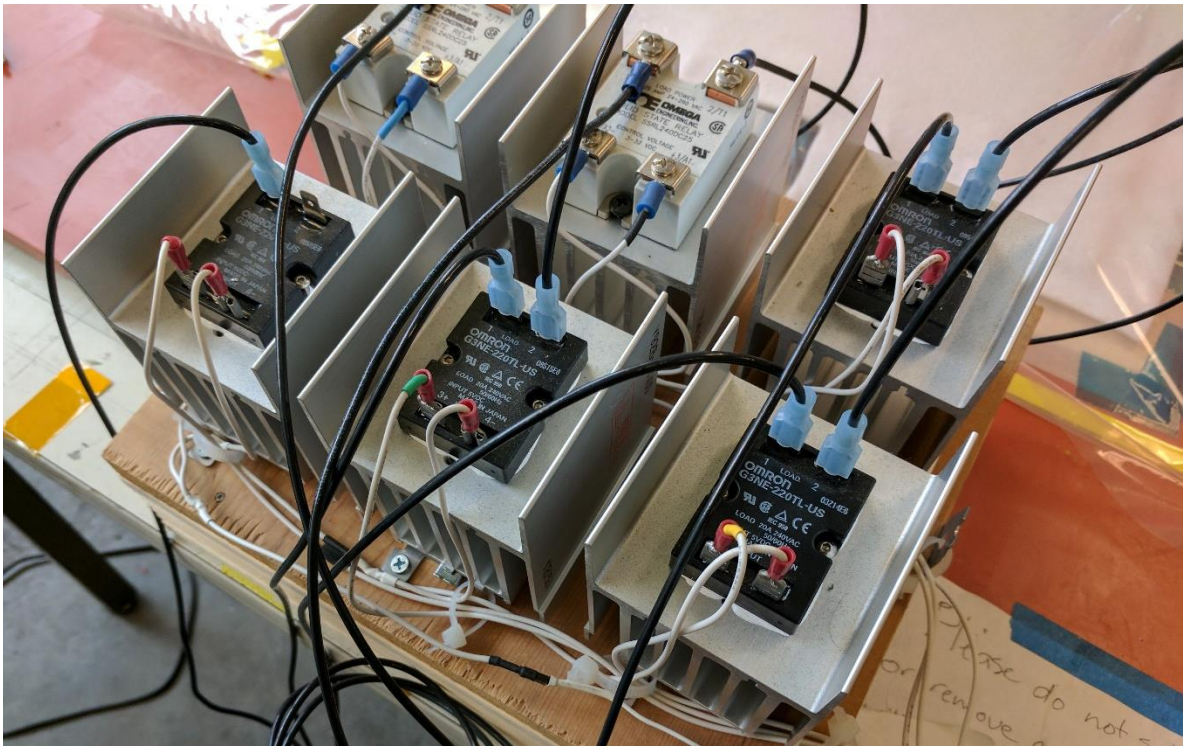


**Fig. A4.** Six of the twelve relays required to control six zones.

## 2. Designing an embedded heater

An embedded heater can be either dry carbon fiber fabric or prepreg. Unidirectional or woven fabric has been used successfully in the past, but the fabric must be thin enough to provide a high resistance. HCS2402-015-05 woven prepreg has been utilized successfully. The orientation of the fabric should be considered when performing multiple tests. All experiments so far have had the current passed parallel to either the warp or the weft of woven fabrics.

When creating the heater ensure that the geometry is rectangular. Only the zone in a rectangular area will be heated uniformly. Once the shape and the size of the area to be heated is determined, add approximately 1.5 in to the dimension perpendicular to the current flow, see the example in Fig. A5. This will reduce the edge effects and ensure the desired heated area has a uniform temperature. Add 0.75 in to the ends of the heater where the terminals will be attached

to the supply power. Apply two layers of copper tape to each end of the embedded heater, perpendicular to the desired current flow (Fig. A6a). Ensure the tape reaches from edge to edge of the heater (Fig. A5). Clamp the taped ends in a vice to ensure they are in full contact with the heater (Fig. A6b).

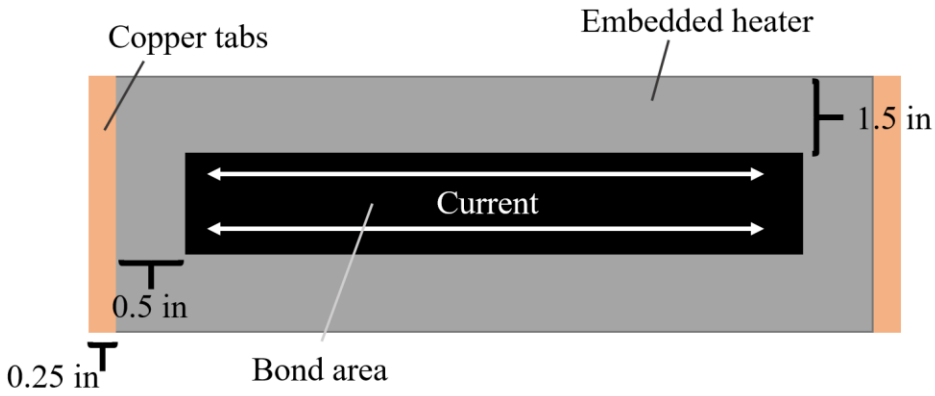


**Fig. A5.** An example embedded heater with copper strips 0.25 in wide on the ends of the heater. The black area is the desired bond area and the grey is added to eliminate edge effects to help ensure uniform bondline temperatures.

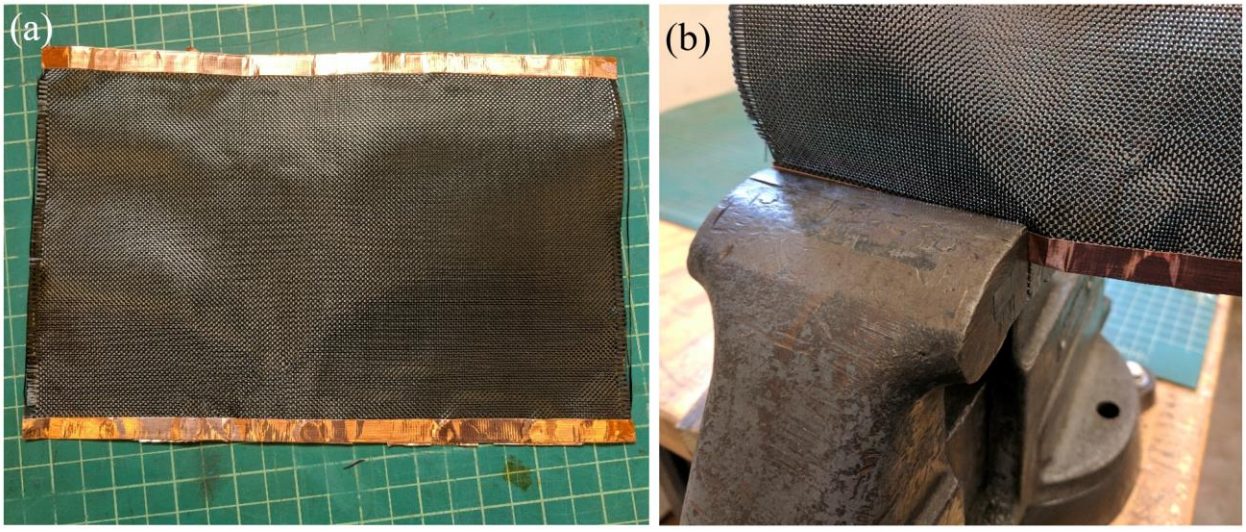


**Fig. A6.** An example embedded heater. (a) After copper tape has been applied. (b) Clamped using a vice to ensure full contact between the copper tape and the fabric.

## 3. Performing a dry run

Thermocouples placed at the bondline are needed to regulate the temperature of the embedded heater while it is curing the adhesive. However, placing thermocouple at the bondline causes an undesirable loss in bond strength. Instead, thermocouples placed outside the bond can be used to control the temperature. The poor thermal conductivities for thick composite parts necessitates that the user estimate the bondline temperature, as the external thermocouples will read temperature values that are significantly lower than those at the bondline. To control using external thermocouples a preliminary test called a dry run is performed with thermocouples placed at the bondline and outside of the part. The thin film adhesive is swapped with a sheet of electrically insulating Teflon and a test performed using the thermocouples at the bondline for control. Once the temperature reaches steady state the temperatures from the thermocouples attached to the outside of the part is noted and used as the set point temperature for future tests. An example of a C-channel bonded to an aircraft skin (a simple sheet of carbon fiber) will be used as a demonstration for the remainder of this document.

### 3.1. Bagging

To perform a dry run, place a layer of bleeder fabric on a rubber caul plate and add a layer of Teflon (Fig. A7a). Apply high-temperature Kapton tape to a central location on the thinnest/flattest adherend on the side that is not to be bonded. This adherend must be flat as any bends in the embedded heater when it is placed overtop can cause temperature spikes. Tape the thermocouple on top of the tape. This ensures that the bead of the thermocouple does not touch the part directly, preventing inaccurate temperature readings. More than one thermocouple may be needed initially to ensure uniform bond temperatures. The thermocouples used in previous tests were type K (approximately 36 gage). Lay the part onto the caul plate with the

thermocouples facing downward. Attach more thermocouples to the side of the part to be bonded in approximately the same location as the thermocouples on the reverse side. These will be the thermocouples used to regulate the bondline temperature. Ensure to insulate the bead of the thermocouples as before so that it does not directly touch the adherend. Note that Teflon wrapped heat sinks can be placed under the embedded heater where the copper tabs are located (Fig. A7b). These are not always necessary but are sometimes needed to prevent temperature spikes when using a relatively large embedded heater. Place a piece of Teflon slightly larger than the embedded heater over the part. This Teflon replicates the thin film adhesive. Place the embedded heater. Apply copper terminals on multiple points of the copper taped area on each end. These terminals should be attached to the relay attached to the power supply. Add a layer of Teflon larger than the embedder heater. Place the second part to be bonded on top (Fig. A7c). Sometimes a stiffener is required for very thin parts to provide even pressure during bonding so that one of the adherends does not press through the electrically insulating adhesive (Fig. A7d). Add a final layer of Teflon (Fig. A7e) and a layer of bleeder fabric. Vacuum bag the setup (Fig. A7f). Ensure that the embedded heater is not creased when bagging as creases lead to hot spots and could not only cause nonuniform temperatures, but damage parts as well. Note that before sealing the part the user should verify that all thermocouples work and there are no problems with the system.

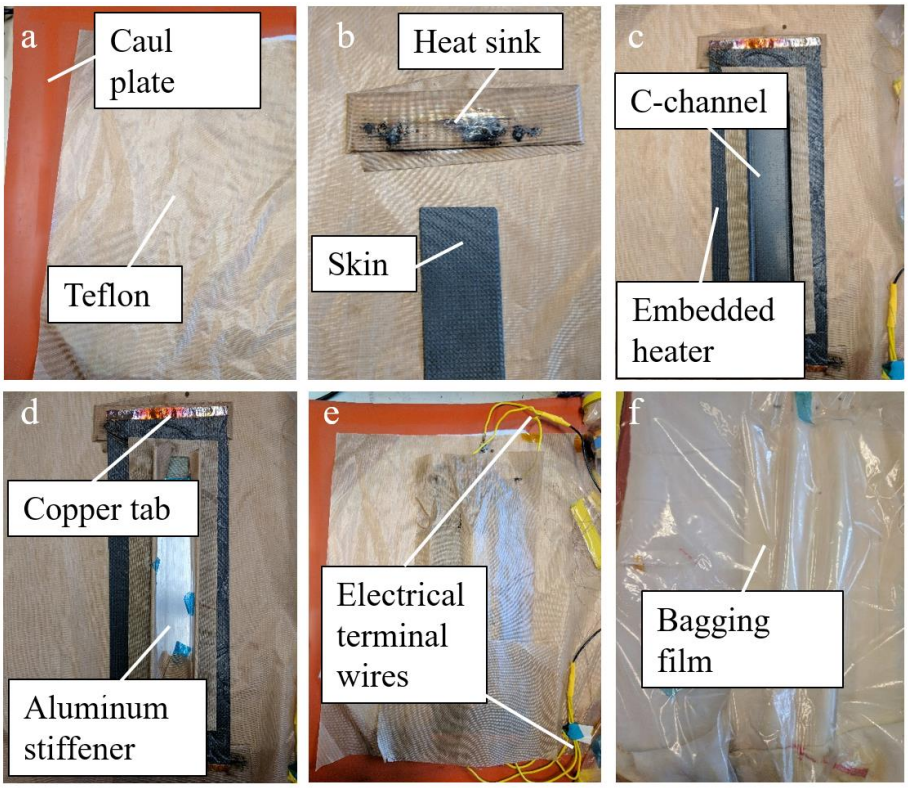


**Fig. A7.** Steps used to bond the adherends. (a) Rubber caul plate with added insulation and Teflon. (b) Added skin and Teflon wrapped copper heat sink. (c) Added Teflon in place of adhesive (during the dry run), embedded heater, Teflon, and then C-channel. (d) Added aluminum stiffener (if needed). (e) Attached copper terminals and added a layer of Teflon. (f) Added bleeder fabric and bagging film and then placed under vacuum.

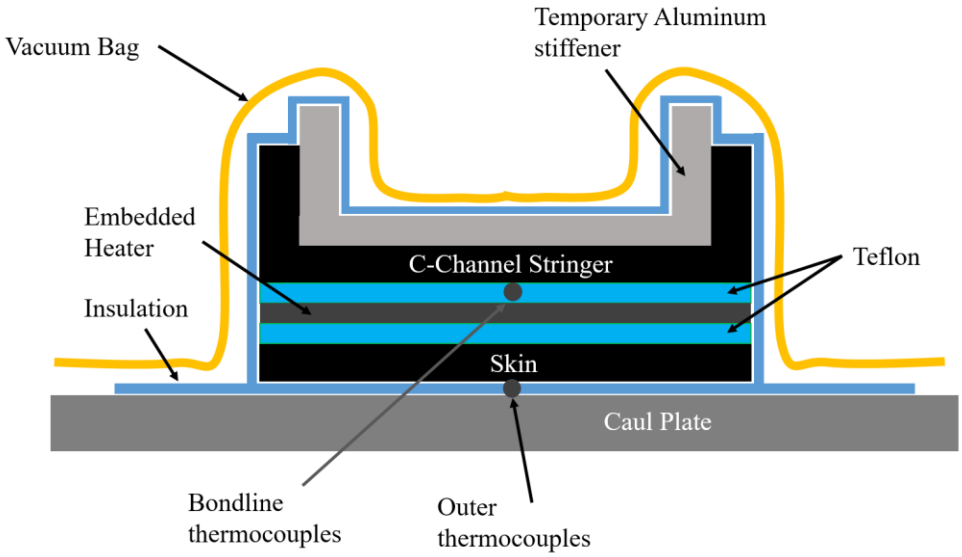


**Fig. A8.** End view of the bagged sample for an example C-channel specimen.

### 3.2. User interface and testing

Once the setup is complete open ‘pwmSlave.ino’ and ‘multiZoneHeater.ino’ using the native Arduino application. These programs should be opened in separate windows. In the ‘multiZoneHeater.ino’ program open the ‘multiZoneHeater.h’ tab. The set point temperature, ramp rate and cure time can be altered in this program (Fig. A9). Upload ‘pwmSlave.ino’ to the slave Arduino that controls the relays and ‘multiZoneHeater.ino’ to the main control Arduino.

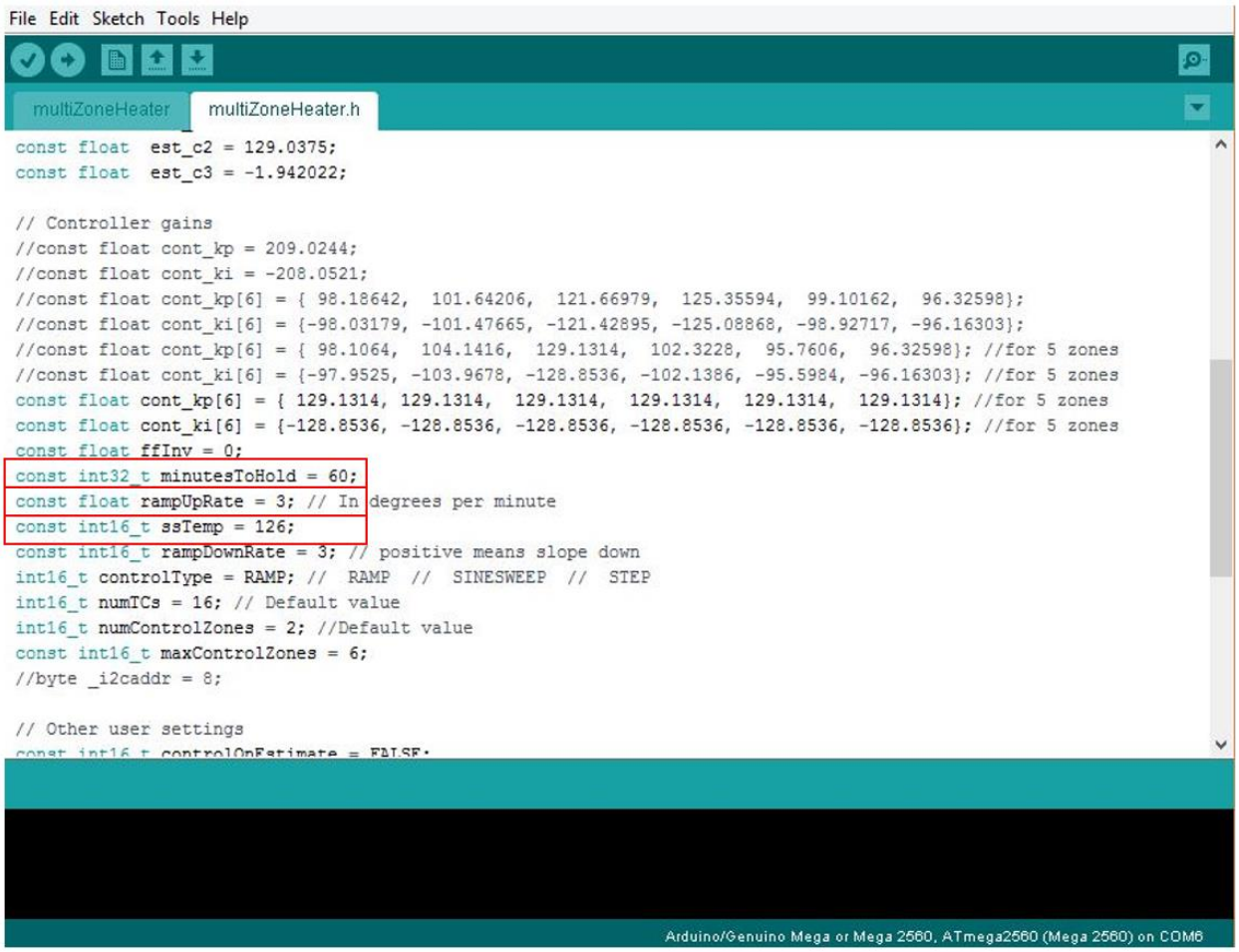


**Fig. A9.** The Main Arduino program used for controlling the temperature. Circled are the ramp rate (°C/min), testing time (min), and set point temperature (°C).

Open ‘MultiZone_OffboardControl.exe’. This is the graphical user interface program needed to observe the test (Fig. A10). Click ‘Connect’. Select the number of thermocouples and zones for the setup. Select the desired thermocouples used to regulate the embedded heater’s temperature (thermocouple 0 is selected by default). Select whether to use the maximum or the average temperature of the controlled thermocouples to determine how the embedded heater is controlled. For the first test, it may be wise to use the maximum temperature in case there are hot spots. Click ‘Save File’ and save the output data to the desired file location. Turn on the power

supply of the embedded heater. To apply current to the embedded heater, click the ‘Controller’ button. By default, the heater temperature will now rise to 127°C at 5°C per minute. These values can only be altered in the Arduino code as explained previously. In the top left hand corner, the ‘Plot Options’ pulldown window allows the user to alter how the temperature information is displayed. When the test is complete click ‘Stop Saving’ and then ‘Controller’. The temperature data will be saved as a ‘.txt’ file which can be uploaded into MATLAB for analysis. To view it in Microsoft Excel, change the extension to ‘.csv’.

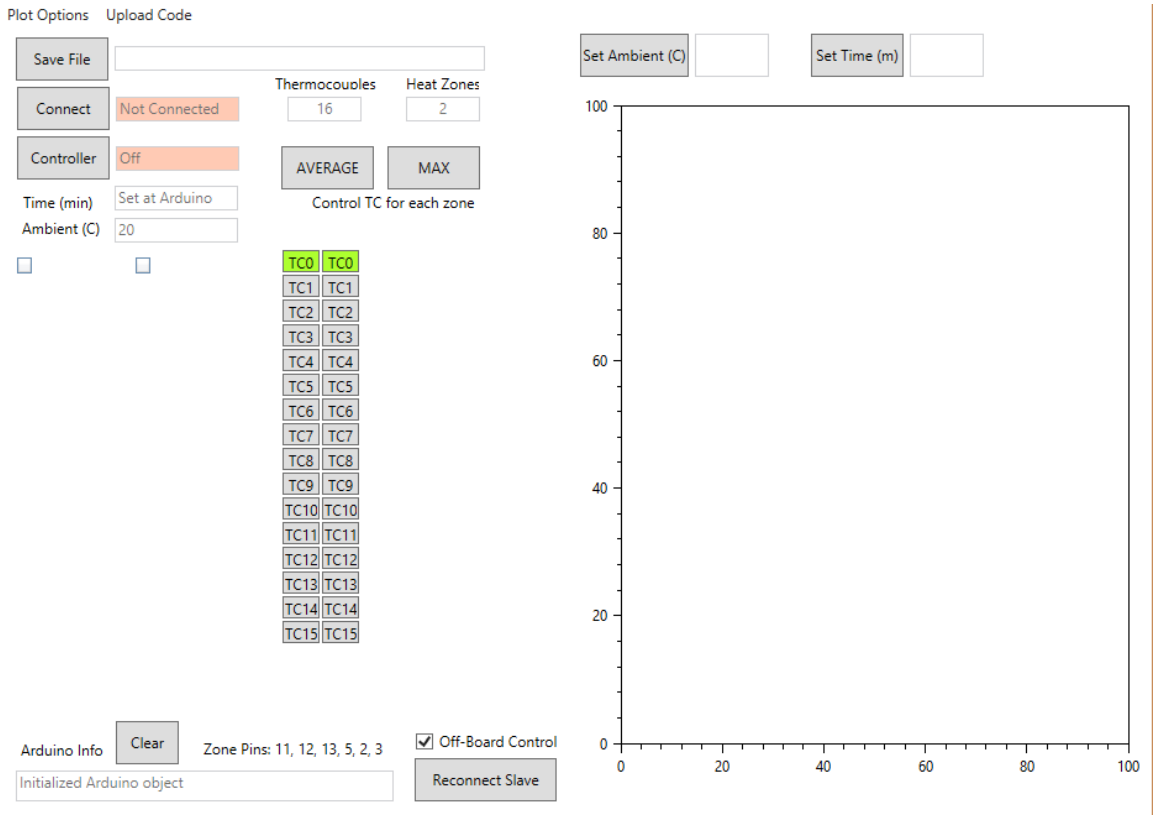


**Fig. A10.** The embedded heater program’s graphical user interface.

When doing a preliminary dry run the thermocouples at the bondline should be used for control. After the test has reached steady state note the external thermocouple temperature and

use it as the new set point temperature for control. Run a second dry run using the external thermocouples for control and confirm that the bond line temperature is as desired.

**4. Performing an actual test**

To perform an actual test simply replace the Teflon sheets with thin film adhesive and remove the thermocouples at the bondline. Use the external thermocouples to control the temperature using the new experimentally determined set point temperature. The dry run section need only be performed once if multiple parts are being bonded, but it should be rerun every time a change is made in the test specimens or how they are bagged.

**5. Multi-zone embedded heaters**

Multi-zone heater setups allow for more versatility than a single zone. They should be used when a uniform temperature cannot be obtained with a single zone setup, such as when there is a heat sink on the back of one of the bonded parts or if the heated area cannot be rectangular.

**6. Potential hazards**

Using this method of heating requires *very* high currents. The user must abide by the following strictures to run a safe experiment.

- Never leave the experiment unattended.
- Ensure that there are no exposed wires outside the vacuum bag.
- Keep the power supply off until a micro-controller is plugged in and the GUI is ready.
- Keep all liquids away from experiment as this has the potential to short.
- Be aware that any electrical shorts can cause over-heating and burning.

- In the event of burning immediately stop the test, turn off the power supply, and air out the room.

7. **Contacts:** Any questions regarding the experimental setup can be directed to the following people:

| | Email |
|---|---|
| Mahdi Ashrafi | me.ashraafi@gmail.com |
| Casey Carte | caseycarte2@gmail.com |
| Brandon Smith | smithbp10@gmail.com |

# Fabric cutter instructions

*Programming the fabric cutter*

1. Remove the prepreg at least one hour before unrolling it to be cut
2. Create a 2D SolidWorks sketch of the cut pattern and save it as a .DXF, note the proper plane orientation
3. Login and open the fabric cutter program on the task bar
4. Click *file*, *new*
5. Click *file*, *import*, and import your .DXF file, ensure that you are using the correct dimensions
6. Place the cut outline in the top window
7. Double click on the center of the box
8. Press Ctrl+A and select the red scissors
9. Click *Done!* In the menu bar
10. Place the cut outline box in the bottom left-hand corner of the large bottom window
11. Ensure that there are no objects on the table
12. Turn on the cutting table power, ensure that the emergency stop is pulled out
13. Unroll the prepreg roll and place plastic on the open parts of the table
14. Press f10 to access the table menu to start
15. Check that the pen is a little higher than the cutting wheel
16. Turn on the vacuum
17. Check to make sure that the pressure is at **maximum 40 psi**
18. Press the glowing button on the table to connect it to the computer and to send the cutting blade to home.

19. Use the pen and the joystick to ensure that the prepreg roll is not skewed and then tape down the end (the vacuum must be turned off to move the prepreg)
20. Note that removing the top layer of plastic from the prepreg can help to remove wrinkles
21. Click the green button near the joystick to begin cutting. If the system stops cutting midway through then it is likely the table has overheated. Wait ten minutes and then press the lit button to continue cutting.
22. After cutting return the blade to the home position by pressing the lit button on the cutter before exiting the program and turning off the table's power

*Changing the fabric cutter blade*

1. Ensure that the table is turned off
2. Simply remove the bolt and remove the old blade
3. Dispose the blade in the sharps container
4. Install the new blade

# MATLAB Code

*Main code to process the raw data*

```
close all
clear all
clc
% Main data analysis

opts = optimset('Display','off'); % used to prevent command line outputs

% ignore first point to calculate
n = 1; %ignore first point
len = 6; % length of the load cycle vector

% % change weather compliance is calculated at Pmax or deltamax
% % at Pmax
% ai1 = 1;
% ai2 = 6;
% at deltamax
ai1 = 2;
ai2 = 7;

S_num = 25; % number of samples

%% Import the raw data

% Example raw data file format for load point displacement (in m) and
% force P (in N)
% data must be a '.csv' file
% Columns are labeled as followed: Load Point Displacement (LPD) for Load
% Cycle (LC) 1, Force for LC 1, LPD for LC 2, Force for LC 2, etc.
% ------------------------------------------------------------------------
% 0       0.227492  0.31    -0.288717   0.69    -0.214137   1.32    -0.02416    1.9    …
% 0.155391    3.07    0.078306

% 0.05  11.199218   0.35    1.979148    0.72    0.827426    1.39    0.797307    1.96    …
% 0.535341    3.09    0.157896

% 0.07  19.087851   0.41    5.96044     0.78    2.337031    1.42    1.159171    1.98    …
% 0.739807    3.12    0.281351

%                   .
%                   .
%                   .
%
% ------------------------------------------------------------------------
```

```
for k=1:S_num
 filename = sprintf('T%d.csv',k);
 slt{k} = csvread(filename);
end

% Example raw data file format for crack growth (in mm)
% data must be a '.csv' file
% The first row is the sample width. The following rows are the crack
% length after each load cycle starting with the initial crack length
% ------------------------------------------------------------------------
% 50.76
% 14.5
% 21.6
% 33.5
% 43.1
% 52.8
% 62.2
% 71.8
% ------------------------------------------------------------------------

for k=1:S_num
 filename = sprintf('c_growth_%d.csv',k);
 crack{k} = csvread(filename);
end

%% Solve for G for all samples and load cycles
for jj = 1:S_num
    slt_w = slt{jj};
    crack_w = crack{jj};
    [G_areas(:,jj), C_s(:,jj), x_s(:,jj), G_fit_s(:,jj), P_s(:,jj),...
        a_s(:,jj),b_s(:,jj), GR(:,jj),a_s2(:,jj), Pm_s(:,jj), yu{jj},...
        G_beams(:,jj), yu_ints(:,jj), m1_s(:,jj)] = ...
        Data_analysis(slt_w, crack_w,ai1,ai2,n);
end


for j = 1:S_num
    yu_1(j) = yu{j}(1,1);
    yu_2(j) = yu{j}(1,2);
    yu_3(j) = yu{j}(1,3);
    yu_4(j) = yu{j}(1,4);
    yu_5(j) = yu{j}(1,5);
    yu_6(j) = yu{j}(1,6);
end
```

```
yu_1avg = abs(mean(yu_ints(1,:)));
yu_2avg = abs(mean(yu_ints(2,:)));
yu_3avg = abs(mean(yu_ints(3,:)));
yu_4avg = abs(mean(yu_ints(4,:)));
yu_5avg = abs(mean(yu_ints(5,:)));
yu_6avg = abs(mean(yu_ints(6,:)));

yu_1std = std(yu_ints(1,:));
yu_2std = std(yu_ints(2,:));
yu_3std = std(yu_ints(3,:));
yu_4std = std(yu_ints(4,:));
yu_5std = std(yu_ints(5,:));
yu_6std = std(yu_ints(6,:));

yu_std = [yu_1std; yu_2std; yu_3std; yu_4std; yu_5std; yu_6std];
yu_avg = [yu_1avg; yu_2avg; yu_3avg; yu_4avg; yu_5avg; yu_6avg];
yu_a_s = [yu_avg yu_std];

%% Summary
close all % optionally close all of the load cycle curves

figure()
hold on
for jj = 1:S_num
    plot(slt{jj}(:,1),slt{jj}(:,2))
    plot(slt{jj}(:,3),slt{jj}(:,4))
    plot(slt{jj}(:,5),slt{jj}(:,6))
    plot(slt{jj}(:,7),slt{jj}(:,8))
    plot(slt{jj}(:,9),slt{jj}(:,10))
    plot(slt{jj}(:,11),slt{jj}(:,12))
end
hold off

title('All samples')
xlabel('Delta (mm)')
ylabel('P (N)')

% Areas Method ----------------------------------------------------

for jj = 1:len
    G_area(jj) = mean(G_areas(jj,:));
    STD_G_area(jj) = std(G_areas(jj,:));
end
G_area_const = mean(G_area);

figure()
```

```
bar(G_area)
hold on
e = errorbar(G_area,STD_G_area,'o')
title('Areas Method')
xlabel('Load Cycle')
ylabel('G (J/m^2)')
e.Marker = '.';
e.MarkerSize = 10;
e.Color = 'red';
e.CapSize = 15;
hold off

% Modified Beam Theory
for jj = 1:len
    G_beam(jj) = mean(G_beams(jj,:));
    STD_G_beam(jj) = std(G_beams(jj,:));
end

figure()
bar(G_beam)
hold on
e = errorbar(G_beam,STD_G_beam,'o')
title('Modified beam theory')
xlabel('Load Cycle')
ylabel('G (J/m^2)')
e.Marker = '.';
e.MarkerSize = 10;
e.Color = 'red';
e.CapSize = 15;
hold off

% Show Compliance spread for the Compliance curve method----------
for jj = 1:len
    C(jj) = mean(C_s(jj,:));
    STD_C(jj) = std(C_s(jj,:));
end

% Calculated average
a_all = a_s(:);
C_all = C_s(:);
ca = [a_all,C_all];
[values, order] = sort(ca(:,1));
ca = ca(order,:);

% % Remove first data set
% ca = ca((S_num+1):length(ca),:);
```

```
% Add zeros at the origin
caz = zeros(S_num,2);
ca = [caz;
    ca];

a_all = ca(:,1);
C_all = ca(:,2);


% Curve fit type

% % First order fit
% F = @(x,a)x(1)*a + x(1);
% x0 = [0.01 -0.0002];

% Second order polynomial fit
F = @(x,a)x(1)*(a.^2) + x(2)*a + x(3);
x0 = [1 1 1];

figure()
[x_all,resnorm,~,exitflag,output] = ...
    lsqcurvefit(F,x0,a_all,C_all,[],[],opts);
fdata = F(x_all,a_all);

hold on
plot(a_all,F(x_all,a_all))
title('Compliance fit')
xlabel('Debond length, a (m)')
ylabel('Compliance, C (m/N)')
for j = 1:S_num
    plot(a_s(:,j),C_s(:,j),'*')
end
% plot(a_all,C_all,'o')
hold off

% Exclude Outliers ------------------------------------------------
cnt = 0;
cas = zeros(length(C_all),2);
for j = 1:length(C_all)
    if abs(fdata(j) - C_all(j)) > 1.5*std(C_all)
        cas(j-cnt,:) = [];
        cnt = cnt + 1;
    else
        cas(j-cnt,:) = ca(j,:);
    end
```

```
end

% Plot the compliance vs a for all samples
figure()
hold on
for j = 1:S_num
   if j < 6
      plot(a_s(:,j),C_s(:,j))
   elseif (5<j)&&(j<11)
      plot(a_s(:,j),C_s(:,j))
   elseif (10<j)&&(j<16)
      plot(a_s(:,j),C_s(:,j))
   elseif (15<j)&&(j<21)
      plot(a_s(:,j),C_s(:,j))
   elseif (20<j)&&(j<26)
      plot(a_s(:,j),C_s(:,j))
   elseif 25 < j
      plot(a_s(:,j),C_s(:,j))
   end
end
xlabel('Debond length, a (m)')
ylabel('Compliance, C (m/N)')
legend('1','2','3','4','5','6','7','8','9','10','11','12','13',...
   '14','15','16','17','18','19','20','21','22','23','24','25',...
   '26','27','28','29','30')
hold off



% Fit a curve to the compliance vs. a data ------------------------------

% average x
for jj = 1:3
   x_avg(jj) = mean(x_s(jj,:));
   STD_x_avg(jj) = std(x_s(jj,:));
end


% Calculate m1 from G_area
for j = 1:6
   m1_w(j) = mean(m1_s(j,:));
end

for j = 1:6
   a_s_w(j) = mean(a_s(j,:));
end
```

```
a_all = a_s(:);
m1_all = m1_s(:);
am1 = [a_all,m1_all];
[values, order] = sort(am1(:,1));
am1 = am1(order,:);

% % Add zeros at the origin
% am1z = zeros(S_num,2);
% am1 = [am1z;
%     am1];

% % First order polynomial
% F = @(x,a)x(1)*(a) + x(2);
% x0 = [1 1];


% Second order polynomial fit
F = @(x,a)x(1)*(a.^2) + x(2)*a + x(3);
x0 = [1 1 1];

% % Third order polynomial fit
% F = @(x,a)x(1)*(a.^3) + x(2)*(a.^2) + x(3)*a+x(4);
% x0 = [1 1 1 1];

[x_m1,resnorm,~,exitflag,output] = ...
    lsqcurvefit(F,x0,am1(:,1),am1(:,2),[],[],opts);

a_use = linspace(0,0.08);
figure()
hold on
plot(am1(:,1),F(x_m1,am1(:,1)))
plot(am1(:,1),am1(:,2),'o')
hold off
xlabel('debond length, a (m)')
ylabel('dC/da')

for jj = 1:S_num
    for j =1:6
        % Second order polynomial fit
        dcda = 2*x_all(1)*(a_s(j,jj))+x_all(2);

        % m1 calculated from G_area, second order
         am = x_m1(1)*((a_s(j,jj))^2)+x_m1(2)*(a_s(j,jj))+x_m1(3);

         % Compliance curve method
```

```
        G_fit(j,jj) = (((P_s(j,jj))^2)/(2*b_s(1,jj)))*dcda;

        % Compliance areas method
        G_fit_area(j,jj) = (((P_s(j,jj))^2)/(2*b_s(1,jj)))*am;
    end
end
G_fit_avgp = G_fit;

% average G calculated using the compliance curve method
for jj = 1:6
    G_fit_avg(jj) = mean(G_fit_avgp(jj,:));
    STD_G_fit_avg(jj) = std(G_fit_avgp(jj,:));
end
figure()
bar(G_fit_avg)
hold on
e = errorbar(G_fit_avg,STD_G_fit_avg,'o')
title('Averaged compliance curve method')
xlabel('Load Cycle')
ylabel('G (J/m^2)')
e.Marker = '.';
e.MarkerSize = 10;
e.Color = 'red';
e.CapSize = 15;
hold off

% average G calculated using the compliance areas method
for jj = 1:6
    G_fit_area_avg(jj) = mean(G_fit_area(jj,:));
    STD_G_fit_area_avg(jj) = std(G_fit_area(jj,:));
end
figure()
bar(G_fit_area_avg)
hold on
e = errorbar(G_fit_area_avg,STD_G_fit_area_avg,'o')
title('Averaged compliance areas method')
xlabel('Load Cycle')
ylabel('G (J/m^2)')
e.Marker = '.';
e.MarkerSize = 10;
e.Color = 'red';
e.CapSize = 15;
hold off

%% Bar plot comparing all methods
```

```
figure()
model_series = [G_area' G_beam' G_fit_avg' G_fit_area_avg'];
model_error = [STD_G_area' STD_G_beam' STD_G_fit_avg' STD_G_fit_area_avg'];
h = bar(model_series);
set(h,'BarWidth',1);    % The bars will now touch each other
set(gca,'YGrid','off')
set(gca,'GridLineStyle','-')
set(get(gca,'XLabel'),'String','Load Cycle')
set(get(gca,'YLabel'),'String','G (J/m^2)')
lh = legend('G_{areas method}','G_{MBT}','G_{C-method derivative}',...
   'G_{C-method area}');
set(lh,'Location','BestOutside','Orientation','horizontal')
hold on;
numgroups = size(model_series, 1);
numbars = size(model_series, 2);
groupwidth = min(0.8, numbars/(numbars+1.5));
for i = 1:numbars
    % Based on barweb.m by Bolu Ajiboye from MATLAB File Exchange
    x = (1:numgroups) - groupwidth/2 + (2*i-1) * groupwidth ...
       / (2*numbars);  % Aligning error bar with individual bar
    errorbar(x, model_series(:,i), model_error(:,i), ...
       'r', 'linestyle', 'none');
end
```

*Function file to be used with the main code*

```
% Function calculates G for all methods for each sample
function [G_area, C, x, G_fit, P, a_s,b, GR,a_s2, Pm, ...
    yu, G_beam, yu_int, m1] = Data_analysis(slt_w, crack_w,ai1,ai2,n)

opts = optimset('Display','off');

% dimensions
b = (crack_w(1))/1000; % m
a0 = (crack_w(2))/1000; %m
a1 = (crack_w(3))/1000; %m
a2 = (crack_w(4))/1000; %m
a3 = (crack_w(5))/1000; %m
a4 = (crack_w(6))/1000; %m
a5 = (crack_w(7))/1000; %m
a6 = (crack_w(8))/1000; %m

a = [a0 a1 a2 a3 a4 a5 a6];
ad = [a1-a0;
    a2-a1;
    a3-a2;
    a4-a3;
    a5-a4;
    a6-a5];

a_s2 = a(1:6);
a = a(1,ai1:ai2);
a = a';
a_s = a;

% import data for each load cycle
test1 = [slt_w(:,1), slt_w(:,2)];
test2 = [slt_w(:,3), slt_w(:,4)];
test3 = [slt_w(:,5), slt_w(:,6)];
test4 = [slt_w(:,7), slt_w(:,8)];
test5 = [slt_w(:,9), slt_w(:,10)];
test6 = [slt_w(:,11), slt_w(:,12)];

% remove zeros that append the relevant values
test = {test1 test2 test3 test4 test5 test6};
for jj  = 1:6
for j = 1:length(test1)
    if test{jj}(j,:) == [0 0]
        if j > 1
```

```
            testr = j;
            break
        end
    end
end
test{jj} = test{jj}(1:testr-1,:);
end


%% Determine the loading curve offset by fitting a line to it

xu = linspace(0,10);
% Second order polynomial fit
F = @(x,a)x(1)*(a.^2) + x(2)*a + x(3);
x0 = [1 1 1];


db = 4; % divide by 7 for unloading curve, 4 for loading curve
figure()
hold on
for jj = 1:6
    if jj == 1
        pointn = length(test{1})/db;
    elseif jj == 2
        pointn = length(test{2})/db;
    elseif jj == 3
        pointn = length(test{3})/db;
    elseif jj == 4
        pointn = length(test{4})/db;
    elseif jj == 5
        pointn = length(test{5})/db;
    elseif jj == 6
        pointn = length(test{6})/db;
    end
%     % unloading curve
%     lena = (length(test{jj})-pointn);
%     lenb = length(test{jj});
    % loading curve
    lena = 1;
    lenb = round(pointn);
    plot(test{jj}(lena:lenb,1),test{jj}(lena:lenb,2),'o')
end
legend('load cycle 1 (precrack)','load cylce 2','load cylce 3',...
    'load cylce 4','load cylce 5','load cylce 6');

for jj = 1:6
```

```
    if jj == 1
        pointn = length(test{1})/db;
    elseif jj == 2
        pointn = length(test{2})/db;
    elseif jj == 3
        pointn = length(test{3})/db;
    elseif jj == 4
        pointn = length(test{4})/db;
    elseif jj == 5
        pointn = length(test{5})/db;
    elseif jj == 6
        pointn = length(test{6})/db;
    end
    % unloading curve
    lena = (length(test{jj})-round(pointn));
    lenb = length(test{jj});
    [xf_w,~,~,~,~] = lsqcurvefit(F,x0,test{jj}(lena:lenb,1),...
        test{jj}(lena:lenb,2),[],[],opts);
    xf_u(jj,:) = xf_w;

    % Second order polynomial fit
    yu_u(:,jj) = xf_u(jj,1).*(xu.^2)+xf_u(jj,2).*xu+xf_u(jj,3);

%     % First order polynomial fit
%     yu(:,jj) = xf(jj,1).*(xu)+xf(jj,2);



    % loading curve
    lena = 1;
    lenb = (length(test{jj})-round(pointn));
%     plot(test{jj}(lena:lenb,1),test{jj}(lena:lenb,2),'o')
    [xf_w,~,~,~,~] = lsqcurvefit(F,x0,test{jj}(lena:lenb,1),...
        test{jj}(lena:lenb,2),[],[],opts);
    xf_l(jj,:) = xf_w;

    % Second order polynomial fit
    yu_l(:,jj) = xf_l(jj,1).*(xu.^2)+xf_l(jj,2).*xu+xf_l(jj,3);

%     % First order polynomial fit
%     yu(:,jj) = xf(jj,1).*(xu)+xf(jj,2);
    plot(xu,yu_l(:,jj));
    yu_int(jj,1) = xf_u(jj,3);

    % Use first point
    delta_offsetu(jj,1) = test{jj}(4,1);
```

```
end

yu = yu_l;
xlabel(' (mm)')
ylabel('P (N)')
hold off



% % Plot the results if desired
% figure()
% hold on
% plot(test1(:,1),test1(:,2));
% plot(test2(:,1),test2(:,2));
% plot(test3(:,1),test3(:,2));
% plot(test4(:,1),test4(:,2));
% plot(test5(:,1),test5(:,2));
% plot(test6(:,1),test6(:,2));
% hold off
% title('Sample 1')
% xlabel('Delta (mm)')
% ylabel('P (N)')
% legend('load cycle 1 (precrack)','load cycle 2','load cycle 3',...
%     'load cycle 4','load cycle 5','load cycle 6');


%% Compliance Curve method to determine G

% Create P (force) and Delta (load point displacement) vectors
[Delta1_max,I1] = max(test1(:,1));
Delta1_max = Delta1_max/1000;
P1 = test1(I1,2); %P @ delta max
P1m = max(test1(:,2)); % P max
P1a = ((test1(I1,2))+(max(test1(:,2))))/2; % P avg=(P max+P @ Delta max)/2
GR1 = (max(test1(:,2)))/(test1(I1,2)); % P max/P @ Delta max

[Delta2_max,I2] = max(test2(:,1));
Delta2_max = Delta2_max/1000;
P2 = test2(I2,2); %P @ delta max
P2m = max(test2(:,2)); % P max
P2a = ((test2(I2,2))+(max(test2(:,2))))/2; % P avg=(P max+P @ Delta max)/2
GR2 = (max(test2(:,2)))/(test2(I2,2)); % P max/P @ Delta max

[Delta3_max,I3] = max(test3(:,1));
Delta3_max = Delta3_max/1000;
P3 = test3(I3,2); %P @ delta max
```

```
P3m = max(test3(:,2)); % P max
P3a = ((test3(I3,2))+(max(test3(:,2))))/2; % P avg=(P max+P @ Delta max)/2
GR3 = (max(test3(:,2)))/(test3(I3,2)); % P max/P @ Delta max

[Delta4_max,I4] = max(test4(:,1));
Delta4_max = Delta4_max/1000;
P4 = test4(I4,2); %P @ delta max
P4m = max(test4(:,2)); % P max
P4a = ((test4(I4,2))+(max(test4(:,2))))/2; % P avg=(P max+P @ Delta max)/2
GR4 = (max(test4(:,2)))/(test4(I4,2)); % P max/P @ Delta max

[Delta5_max,I5] = max(test5(:,1));
Delta5_max = Delta5_max/1000;
P5 = test5(I5,2); %P @ delta max
P5m = max(test5(:,2)); % P max
P5a = ((test5(I5,2))+(max(test5(:,2))))/2; % P avg=(P max+P @ Delta max)/2
GR5 = (max(test5(:,2)))/(test5(I5,2)); % P max/P @ Delta max

[Delta6_max,I6] = max(test6(:,1));
Delta6_max = Delta6_max/1000;
P6 = test6(I6,2); %P @ delta max
P6m = max(test6(:,2)); % P max
P6a = ((test6(I6,2))+(max(test6(:,2))))/2; % P avg=(P max+P @ Delta max)/2
GR6 = (max(test6(:,2)))/(test6(I6,2)); % P max/P @ Delta max

GR = [GR1; GR2; GR3; GR4; GR5; GR6];
Pm = [P1m P2m P3m P4m P5m P6m]; % P max
Pa = [P1a P2a P3a P4a P5a P6a]; % P avg
P = [P1 P2 P3 P4 P5 P6];

% % Add an offset to P to make G more in line with the areas method
% % P offset for every load cycle
% for j = 1:length(P)
%     P(j) = P(j)+yu_int(j);
% end
Delta = [Delta1_max Delta2_max Delta3_max ...
    Delta4_max Delta5_max Delta6_max];
% Delta offset using loading curve
for j = 1:6
    delta_w(j) = Delta(j)-(delta_offsetu(j)/1000);
end

% delta_w(6) = Delta(6)-(delta_offsetu(5)/1000);
Delta = delta_w;

% P = Pm; % P max
```

```
% P = Pa; % P avg
hu = 0; % load point displacement offset if desired
c1 = (Delta(1)-hu)/P(1);
c2 = (Delta(2)-hu)/P(2);
c3 = (Delta(3)-hu)/P(3);
c4 = (Delta(4)-hu)/P(4);
c5 = (Delta(5)-hu)/P(5);
c6 = (Delta(6)-hu)/P(6);
C = [c1 c2 c3 c4 c5 c6]; % Compliance vector
C = C';

if n == 1

% Create an equation to fit to the compliance data
% Second order polynomial fit
F = @(x,a)x(1)*(a.^2) + x(2)*a + x(3);
x0 = [1 1 1];

% % Power fit
% F = @(x,a)x(1)*(a.^(x(2)));
% x0 = [1 1];

[x,resnorm,~,exitflag,output] = lsqcurvefit(F,x0,a,C,[],[],opts);


% Calculating G
for jj = 1:6
   dcda = 2*x(1)*(a(jj))+x(2); % Second order polynomial fit
%     dcda = x(2)*x(1)*(a(jj).^(x(2))); % Power fit
   G_fit(jj) = ((P(jj)^2)/(2*b))*dcda;
end

% % plot G for a single load cycle
% figure()
% bar(G_fit)

%% Areas Method
test = {test1 test2 test3 test4 test5 test6};
I = [I1 I2 I3 I4 I5 I6];
for jj = 1:6
   testw = test{jj};
%energy loading
e_load(1,1)= 0;
for j = 2:length(testw(:,1))
   if j <= I(jj)
      testu = [testw(j-1,2) testw(j,2)];
```

```
        e_load(j-1,1) = (mean(testu)*(testw(j,1)-testw(j-1,1)))/1000;
    else
        e_load(j-1,1) = 0;
    end
end

%energy unloading
e_uload(1,1)= 0;
for j = 2:length(testw(:,1))
    if j > I(jj)
        testu = [testw(j-1,2) testw(j,2)];
        e_uload(j-1,1) = (mean(testu)*(testw(j,1)-testw(j-1,1)))/1000;
    else
        e_uload(j-1,1) = 0;
    end
end

G1_area = (sum(e_load)+sum(e_uload))/(b*ad(jj));

G_area(jj) =  G1_area;

end

% caluclate m1 from G_area
for j = 1:6
    m1(j) = (G_area(j)*2*b)/((P(j)^2));
end

%% Modified beam theory

% Line fit
F = @(x,a)x(1)*(a) + x(2);
x0 = [1 1];

[xb,resnorm,~,exitflag,output] = lsqcurvefit(F,x0,a,(C.^(1/3)),[],[],opts);
delta_a = abs(-xb(2)/xb(1));
for jj = 1:6
    G_beam(jj,1) = (3*(P(jj)+0)*Delta(jj))/(2*b*(a(jj)+delta_a));
end



end
```